Dynamics of Ribonuclease H: Temperature Dependence of Motions on Multiple Time Scales†

Arthur M. Mandel, Mikael Akke, and Arthur G. Palmer, III*

Department of Biochemistry and Molecular Biophysics, Columbia University, 630 West 168th Street, New York, New York 10032

Received August 19, 1996; Revised Manuscript Received October 22, 1996⊗

ABSTRACT: The temperature dependence of the backbone motions in *Escherichia coli* ribonuclease HI was studied on multiple time scales by ^{15}N nuclear magnetic spin relaxation. Laboratory frame relaxation data at 285, 300, and 310 K were analyzed using the model-free and reduced spectral density approaches. The temperature dependence of the order parameters was used to define a characteristic temperature for the motions of the backbone N−H bond vectors on picosecond to nanosecond time scales. The characteristic temperatures for secondary structure elements, loops, and the C-terminus are ∼1000, ∼300, and ∼170 K, respectively. The observed variation in the characteristic temperature indicates that the energy landscape, and thus the configurational heat capacity, is markedly structure dependent in the folded protein. The effective correlation times for internal motions do not show significant temperature dependence. Conformational exchange was observed for a large number of residues forming a contiguous region of the protein that includes the coiled coil formed by helices α_A and α_D. Exchange broadening in the CPMG experiments decreased with increased temperature, directly demonstrating that the microscopic exchange rate is faster than the pulse repetition rate of 1.2 ms. The temperature dependence of the exchange contributions to the transverse relaxation rate constant shows approximately Arrhenius behavior over the studied temperature range with apparent activation enthalpies of ∼20−50 kJ/mol. Numerical calculations suggest that these values underestimate the activation barriers by at most a factor of 2. The present results obtained at 300 K are compared to those reported previously [Mandel, A. M., Akke, M., & Palmer, A. G., III (1995) *J. Mol. Biol. 246,* 144−163] to establish the reproducibility of the experimental techniques.

Ribonuclease HI (RNase H, EC 3.1.26.4) is an ubiquitous endonuclease that hydrolyzes the RNA strand in RNA−DNA hybrid molecules (Stein & Hausen, 1969; Crouch & Dirksen, 1982; Crouch, 1990; Wintersberger, 1990). RNase H appears to participate in various aspects of DNA replication in diverse retroviral, procaryotic, and eucaryotic organisms. *Escherichia coli* RNase H inhibits replication from sites other than oriC (de Massy et al., 1984; Horiuchi et al., 1984) and removes Okazaki fragments during lagging strand synthesis (Kitani et al., 1985). During reverse transcription of the viral genome, the RNase H domain of reverse transcriptase cleaves the $tRNA^{Lys3}$ primer required for minus strand synthesis (Gilboa et al., 1979; Omer & Faras, 1982; Furfine & Reardon, 1991; Smith & Roth, 1992), degrades the RNA template during or after minus strand synthesis (Mölling et al., 1971), and removes the polypurine RNA primer during or after plus strand synthesis (Champoux et al., 1984; Huber & Richardson, 1990). RNase H enzymes share sequence and structural similarity (Doolittle et al., 1989). For example, *Thermus thermophilus* RNase H and the C-terminal RNase H domain of human immunodeficiency virus (HIV) retroviral reverse transcriptase have 52% and 24% sequence identity with *E. coli* RNase H (Crouch, 1990) and strong structural homology (Davies et al., 1991; Ishikawa et al., 1993c).

E. coli RNase H is a single-chain polypeptide of 155 residues and M_r = 17 600. Its three-dimensional structure has been determined by X-ray crystallography (Katayanagi et al., 1990; Yang et al., 1990a; Katayanagi et al., 1992) and nuclear magnetic resonance (NMR)[1] spectroscopy (Yamazaki et al., 1993). As shown in Figure 1, RNase H is an α/β beta protein with five α-helices, denoted α_A to α_E , and a five-stranded β-sheet, denoted β_1 to β_5. The region between α_C and α_D (residues 90−99) has been termed the handle region (Yang et al., 1990a), while the overlapping region from residues 81 to 99 (including α_C) has been termed the basic protrusion (Katayanagi et al., 1990). Mutagenesis has implicated three invariant residues, Asp 10, Glu 48, and Asp 70, which are located in a concave depression in the three-dimensional structure of the protein, as essential to catalytic function (Kanaya et al., 1990). In addition, four highly conserved residues, Ser 71, His 124, Asp 130, and Asp 134, are clustered near the catalytic residues. Loops between β_1 and β_2, between α_C and α_D (the handle), and between β_5 and α_E have been suggested to participate in substrate binding on the basis of mutagenesis (Oda et al., 1993b), NMR spectroscopy (Nakamura et al., 1991; Oda et al., 1993a), and model building (Yang et al., 1990a; Nakamura et al., 1991; Katayanagi et al., 1992). A putative binding site for a substrate phosphate group has been

† This work was supported by grants to A.G.P. from the Searle Foundation and the National Institutes of Health (GM-50291). A.M.M. was supported by a National Institutes of Health M.S.T.P. grant (5T32-GM-07367). M.A. was supported by a postdoctoral fellowship from the Swedish Natural Sciences Research Council and a travel grant from the Swedish Medical Research Council.

⊗ Abstract published in *Advance ACS Abstracts,* December 1, 1996.

[1] Abbreviations: CPMG, Carr−Purcell−Meiboom−Gill; HIV, human immunodeficiency virus; HSQC, heteronuclear single-quantum coherence; HSVD, Hankel singular value decomposition; NMR, nuclear magnetic resonance; NOE, nuclear Overhauser effect; NOESY, NOE spectroscopy; TOCSY, total correlation spectroscopy; PDB, protein data bank.

S0006-2960(96)02089-2 CCC: $12.00

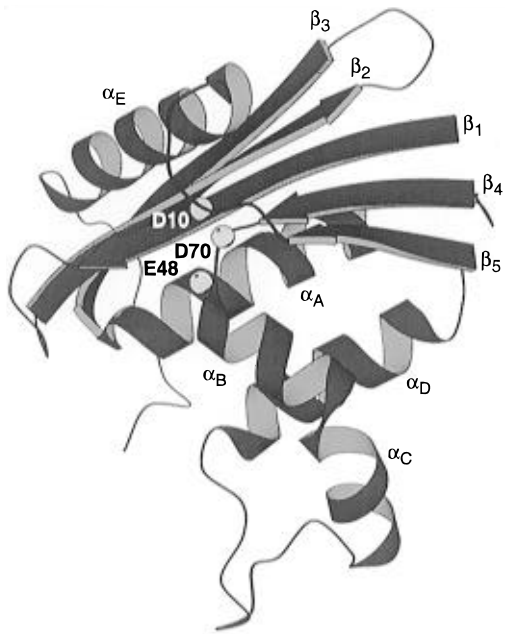

FIGURE 1: Structure of *E. coli* RNase H. RNase H is an α/β protein with five α-helices, denoted α_A to α_E (residues 43−58, 71−80, 81−88, 100−112, and 127−142), and a five-stranded β-sheet, denoted β_1 to β_5 (residues 4−13, 18−27, 32−42, 64−69, and 115−120) with topology 3↓ 2↑ 1↓ 4↓ 5↓. The active site residues are shown as spheres. The figure was drawn with the program MOLSCRIPT (Kraulis, 1991) using the PDB coordinate file 1RNH.

identified 13.7 Å from the catalytic site at the N-termini of α_A and α_D (Yang et al., 1990a). As demonstrated by NMR spectroscopy (Oda et al., 1991) and X-ray crystallography (Katayanagi et al., 1990, 1992, 1993), RNase H has at least one metal cation binding site, involving side chains of Asn 44 and Glu 48, located near the loop between β_1 and β_2. The stability of *E. coli* RNase H has been explored by substituting *T. thermophilus* sequences into the *E. coli* protein sequence (Kimura et al., 1992a,b) and by other designed mutations (Ishikawa et al., 1993a,b). The folding pathway of RNase H has been investigated by NMR hydrogen exchange measurements (Yamasaki et al., 1995a; Chamberlain et al., 1996) and by examination of acid-destabilized states of the molecule (Dabora & Marqusee, 1994).

Measurements of nuclear spin relaxation in isotopically enriched proteins by NMR spectroscopy is a powerful method for the study of intramolecular conformational dynamics (Palmer, 1993; Wagner, 1993; Palmer et al., 1996). In the most common approach, ^{15}N spin relaxation rate constants are measured, while ^{13}C spin relaxation is utilized less frequently (Palmer et al., 1991; Mispelter et al., 1995; Wand et al., 1996). Recently, promising ^{2}H spin relaxation techniques have been reported (Muhandiram et al., 1995). A variety of techniques have been developed to interpret spin relaxation measurements in terms of intramolecular dynamic processes: the Lipari−Szabo model-free formalism (Lipari & Szabo, 1982a), the extended two-time-scale model (Clore et al., 1990b), spectral density mapping (Peng & Wagner, 1992), and reduced spectral density analysis (Farrow et al., 1995; Ishima & Nagayama, 1995). Experimental studies can be complemented by long (∼1 ns) solvated molecular dynamics simulations (Philippopoulos & Lim, 1995). These experimental and theoretical studies have provided great insight into the amplitudes and time scales of intramolecular dynamics on both the picosecond to nanosecond and the microsecond to millisecond time scales and are beginning to correlate motions on these time scales with biological function (Palmer et al., 1996).

A comprehensive understanding of intramolecular dynamical modes in proteins necessitates characterization of the energetics and mechanisms of motions as well as time scales and amplitudes. The temperature dependence of internal motional processes contains important information on the energetics of the dynamical processes and imposes constraints on possible mechanisms. Protein structure and function are strongly temperature dependent, and this sensitivity may result in part from internal dynamic processes (Gurd & Rothgeb, 1979; Frauenfelder et al., 1991). Optical spectroscopy (Frauenfelder et al., 1988) and X-ray crystallography (Tilton et al., 1992) have provided rich insights into the temperature dependence of protein dynamics and have provided the primary experimental evidence for the existence "conformational substates" in proteins. Investigation of the temperature dependence of nuclear spin relaxation has a long history (Kowalewski, 1989, 1991); nonetheless, the powerful heteronuclear NMR spectroscopic techniques currently available have not been used to investigate the temperature dependence of conformational dynamics in proteins.

Previously, we described the dynamics of *E. coli* RNase H at 300 K as derived from ^{15}N spin relaxation measurements at 11.7 T (Mandel et al., 1995). This study revealed that RNase H has complex intramolecular dynamical properties; in particular, motions on multiple time scales were observed in the coiled coil formed by helices α_A and α_D, in the putative substrate binding loops, and in the handle region. More recently, a similar study performed at 14.0 T has been reported (Yamasaki et al., 1995b). In addition, solvated molecular dynamics simulations of RNase H have been performed in order to evaluate dynamic properties of catalytically important residues that could not be quantified experimentally and to explain the physical basis for the experimental results (Philippopoulos & Lim, 1995; Yamasaki et al., 1995b).

In the present study, the temperature dependence of conformational dynamics on both picosecond to nanosecond and microsecond to millisecond time scales in RNase H is characterized from ^{15}N spin relaxation rate constants measured at 285, 300, and 310 K. In addition, the present results at 300 K are compared with prior experimental NMR results in order to establish the reproducibility of these techniques.

THEORY

Relaxation of amide ^{15}N nuclei is dominated by the dipolar interaction with the directly attached ^{1}H spin and by the chemical shift anisotropy mechanism. Relaxation parameters are given by (Abragam, 1961)

$$R_1 = (d^2/4)[J(\omega_H-\omega_N) + 3J(\omega_N) + 6J(\omega_H+\omega_N)] + c^2J(\omega_N) \quad (1)$$

$$R_2 = (d^2/8)[4J(0) + J(\omega_H-\omega_N) + 3J(\omega_N) + 6J(\omega_H) + 6J(\omega_H+\omega_N)] + (c^2/6)[4J(0) + 3J(\omega_N)] + R_{ex} \quad (2)$$

$$\mathrm{NOE} = 1 + (d^2/4R_1)(\gamma_H/\gamma_N)[6J(\omega_H+\omega_N) - J(\omega_H-\omega_N)] \quad (3)$$

in which $d = \mu_0 h\gamma_N\gamma_H\langle r_{NH}^{-3}\rangle/(8\pi^2)$; $c = \omega_N\Delta\sigma/\sqrt{3}$; μ_0 is the permeability of free space; h is Planck's constant; γ_H and γ_N are the gyromagnetic ratios of ^{1}H and ^{15}N, respectively; $r_{NH} = 1.02$ Å is the nitrogen−hydrogen bond length; ω_H and ω_N are the Larmor frequencies of ^{1}H and ^{15}N, respectively; and $\Delta\sigma = -160$ ppm is the chemical shift anisotropy measured for ^{15}N nuclei in helical polypeptide chains (Hiyama et al., 1988). The model-free formalism, as described by Lipari and Szabo (1982a,b) and extended by Clore and co-workers (Clore et al., 1990b), determines the amplitudes and time scales of the intramolecular motions by modeling the spectral density function, $J(\omega)$, as

$$J(\omega) = \frac{2}{5}\left[\frac{S^2\tau_m}{1+(\omega\tau_m)^2} + \frac{(1-S_f^2)\tau'_f}{1+(\omega\tau'_f)^2} + \frac{(S_f^2-S^2)\tau'_s}{1+(\omega\tau'_s)^2}\right] \quad (4)$$

in which $\tau'_f = \tau_f\tau_m/(\tau_f+\tau_m)$, $\tau'_s = \tau_s\tau_m/(\tau_s+\tau_m)$, τ_m is the isotropic rotational correlation time of the molecule, τ_f is the effective correlation time for internal motions on a fast time scale defined by $\tau_f < 100-200$ ps, τ_s is the effective correlation time for internal motions on a slow time scale of ~1 ns defined by $\tau_f < \tau_s < \tau_m$, $S^2 = S_f^2S_s^2$ is the square of the generalized order parameter characterizing the amplitude of the internal motions, and S_f^2 and S_s^2 are the squares of the order parameters for the internal motions on the fast and slow time scales, respectively. Generalized order parameters represent motions that are described by dynamics on the picosecond to nanosecond time scale, with values ranging from zero for isotropic internal motions to unity for completely restricted motion in a molecular reference frame.

Akke et al. (1993) have demonstrated that the statistical mechanical partition function for motions of an N−H bond vector and the associated Gibbs free energy can be estimated from experimental order parameters. Yang and Kay (1996) have utilized this approach to calculate the thermodynamic entropy for a number of quantum mechanical and classical partition functions and have demonstrated that simple model partition functions accurately reproduce entropies calculated from molecular dynamics simulations. In the following, a simple derivation is used to indicate the general form and magnitude of the temperature dependence; a more detailed derivation will be given elsewhere. The order parameter, S^2, is given by (Lipari & Szabo, 1982a; Henry & Szabo, 1985; Brüschweiler & Wright, 1994)

$$S^2 = \sum_{m=-2}^{2}\langle Y_2^m{}^*(\Omega)\rangle\langle Y_2^m(\Omega)\rangle = 1 - \sum_{m=-2}^{2}\sigma_{2m}^2 \quad (5)$$

in which $Y_2^m(\Omega)$ are modified spherical harmonic functions (Brink & Satchler, 1968), $\Omega = (\theta, \phi)$ defines the orientation of the N−H vector in a molecular reference frame, σ_{2m}^2 is the variance in the expectation value of $Y_2^m(\Omega)$, and angular brackets indicate ensemble averaging. The derivative dS^2/dT is simply

$$\frac{dS^2}{dT} = -\sum_{m=-2}^{2}\frac{d\sigma_{2m}^2}{dT} \quad (6)$$

which, in principle, can be calculated from statistical mechanical considerations. A number of potential energy functions have been presented for analysis of order parameters in terms of the partition function (Akke et al., 1993; Yang & Kay, 1996). If the N−H bond vectors are restricted to small excursions within an axially symmetric parabolic potential, $E(\theta)/(k_BT) = \theta^2T^*/T$ (which may be regarded as the first term of an expansion), then

$$S = \langle Y_2^0(\Omega)\rangle = 1 - \frac{3}{2}\langle\theta^2\rangle \quad (7)$$

$$\langle\theta^2\rangle = \frac{\int\theta^2\exp[-\theta^2T^*/T]\sin\theta\,d\theta}{\int\exp[-\theta^2T^*/T]\sin\theta\,d\theta} = \frac{T}{T^*} \quad (8)$$

$$\frac{d(1-S)}{dT} = \frac{3}{2}\frac{d}{dT}\langle\theta^2\rangle = \frac{3}{2T^*} \quad (9)$$

in which k_B is Boltzmann's constant and T^* defines a characteristic temperature for the dynamical process. The characteristic temperature describes the density of energy states thermally accessible to the bond vector (*vide infra*). As shown by eqs 6−9, order parameters are expected to decrease with increasing temperature, and the increased accessible conformational space reflects an increase in absolute entropy. The temperature dependence of order parameters provides a strong constraint on proposed potential energy functions and therefore aids in characterizing the energy landscapes of proteins.

Internal correlation times are measured less precisely than order parameters in ^{15}N relaxation experiments and are difficult to interpret quantitatively. The temperature dependence of the internal correlation times depends on whether the microscopic dynamic processes are characterized by activated, diffusional, power law or other kinetic models. Herein, a simple phenomenological temperature dependence, $\tau_e^{-1} = \tau_0^{-1}\exp(-E_a/k_BT)$, in which τ_0 is the correlation time at infinite temperature and E_a is an activation energy, is assumed.

A phenomenological exchange term, R_{ex}, is included in eq 2 to account for chemical-exchange processes that contribute to the decay of transverse magnetization during the CPMG pulse train in the experiment used to measure R_2 (Bloom et al., 1965; Wennerström, 1972). The following expression approximates the effect of two-site chemical exchange in a CPMG experiment (Luz & Meiboom, 1963):

$$R_{ex} = \frac{p_1p_2(\Delta\omega)^2}{k_{ex}}\left[1 - \frac{2}{k_{ex}\tau_{cp}}\tanh\left(\frac{k_{ex}\tau_{cp}}{2}\right)\right] \quad (10)$$

in which $\tau_{cp} = 1.2$ ms is the delay between 180° pulses in the CPMG sequence, $\Delta\omega$ is the difference in chemical shift of the nucleus in the two conformational states, $k_{ex} = k_{-1}/p_1 = k_1/p_2$, $1 \geq p_1 \geq 0.5$ and $p_2 = (1-p_1)$ are the populations of the two conformational states, k_1 is the forward exchange rate constant, and k_{-1} is the reverse exchange rate constant. The dependence of R_{ex} on k_{ex} is shown in Figure 2. This equation is in close agreement with exact formulations (Allerhand & Gutowsky, 1965); numerical calculations

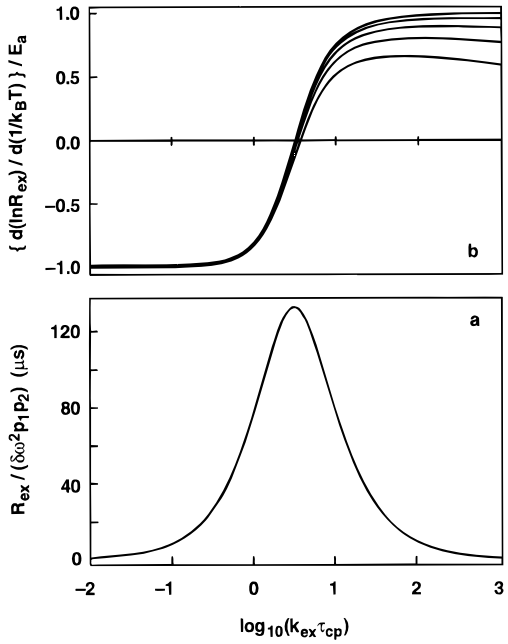

FIGURE 2: Chemical exchange contributions in CPMG experiments. (a) The dependence of the phenomenological exchange rate constant, R_{ex}, on the microscopic kinetic rate constant, k_{ex}, is illustrated for two-site exchange and arbitrary populations. The spacing between 180° pulses in the CPMG experiment is τ_{cp}. (b) The relative accuracy of apparent activation barriers derived from $\ln R_{ex}$ versus $1/T$ is shown as a function of the dimensionless parameter $k_{ex}\tau_{cp}$. Individual curves are given for populations p_1 of 0.5, 0.6, 0.7, 0.8, and 0.9 (from bottom to top).

comparing eq 10 with the exact equation (Jen, 1978; Davis et al., 1994) indicate that, for exchange parameters anticipated for ^{15}N nuclei in proteins ($\Delta\omega < 4$ ppm; $k_{ex}\tau_{cp} > 10^{-2}$), eq 10 is accurate to within 5%. The apparent exchange rate constant is a maximum for $k_{ex}\tau_{cp} = 3.2$; for slow exchange, $k_{ex}\tau_{cp} \ll 3.2$, R_{ex} approaches zero; and for fast exchange, $k_{ex}\tau_{cp} \gg 3.2$, $R_{ex} = p_1p_2(\Delta\omega)^2/k_{ex}$, which is identical to free precession exchange broadening. Exchange processes result in detectable dephasing of the resonance signal if k_{ex} is within approximately 2 orders of magnitude of $3.2/\tau_{cp} = 2.7 \times 10^3$ s^{-1}, and only if $\Delta\omega > 0$. Thus, R_{ex} terms represent conformational exchange processes that can be described on the microsecond to millisecond time scale. Values of R_{ex} obtained at a single magnetic field strength and a single temperature normally cannot be analyzed quantitatively because the populations and chemical shifts of the conformational states usually are unknown.

The temperature dependence of R_{ex} arises through the Arrhenius equation $k_1 = k_1^0\exp[-E_a/(k_BT)]$ and the Boltzmann distribution $p_1 = \{1 + \exp[-\Delta G/(k_BT)]\}^{-1}$, in which k_1^0 is a preexponential factor, E_a is the activation energy, and ΔG is the difference in free energy between conformational states 1 and 2. Increasing T increases k_{ex} because $E_a > \Delta G$ by construction. If $k_{ex} > 3.2/\tau_{cp}$, then increasing T decreases R_{ex}; conversely if $k_{ex} < 3.2/\tau_{cp}$, then increasing T increases R_{ex}. Thus, the sign of dR_{ex}/dT immediately indicates whether the microscopic exchange rate is faster or slower than $3.2/\tau_{cp}$. In general, $d\ln R_{ex}/d(1/T) \leq |E_a|$, both due to the dependence of p_1 on T and due to the effect of the pulsing rate. Numerical calculations given in Figure 2 indicate that, for $k_{ex} > 10/\tau_{cp}$, apparent activation barriers derived from the slope of plots of $\ln R_{ex}$ versus $1/T$ underestimate E_a by less than a factor of 2.

The model-free formalism utilized herein assumes that overall rotational diffusion is isotropic. Recent work has shown that rotational diffusion anisotropy of proteins can be characterized from ^{15}N relaxation rate constants by direct fitting of R_2/R_1 ratios (Tjandra et al., 1995; Zheng et al., 1995) or by fitting local diffusion constants (Brüschweiler et al., 1995). In the latter approach, a local diffusion constant, $D_i = (6\tau_{mi})^{-1}$, for the ith residue is determined from the R_2/R_1 ratio by using eqs 1, 2, and 4 under the conditions $S_s^2 = 1$ and $\tau_f \rightarrow 0$. As described in more detail elsewhere (Brüschweiler et al., 1995; Lee et al., 1996), the diffusion tensor is determined by solution of the equation:

$$D_i = \mathbf{e}_i^{\mathrm{T}}\mathbf{A}\mathbf{D}\mathbf{A}^{-1}\mathbf{e}_i \qquad (11)$$

in which $\mathbf{e}_i$ is the unit vector defining the orientation of the ith N−H bond vector, **A** is the transformation matrix relating the molecular reference frame (defined by the molecular coordinate frame of the PDB file 1RNH) and the reference frame defined by the principal axes of the diffusion tensor, **D** is a diagonal matrix with values $(D_{yy} + D_{zz})/2$, $(D_{xx} + D_{zz})/2$, and $(D_{xx} + D_{yy})/2$, and D_{xx}, D_{yy}, and D_{zz} are the three diffusion constants for a fully anisotropic diffusion tensor. For an axially symmetric diffusion tensor, $D_{xx} = D_{yy} = D_\perp$ and $D_{zz} = D_{||}$. For a spherically symmetric diffusion tensor, $D_{xx} = D_{yy} = D_{zz} = D_{iso}$.

As an alternative to the model-free approach, values of the spectral density function at three frequencies, $\omega = 0$, ω_N, and $0.870\ \omega_H$, can be determined directly from the three measured relaxation parameters by using the reduced spectral density formalism (Farrow et al., 1995; Ishima & Nagayama, 1995). In this approach, simplified expressions for the ^{15}N relaxation parameters are obtained from eqs 1, 2, and 3 by assuming that $dJ(\omega)/d\omega$ is smooth between $\omega = \omega_H + \omega_N$ and $\omega = \omega_H - \omega_N$.

$$R_1 = (d^2/4)[3J(\omega_N) + 7J(0.921\omega_H)] + c^2J(\omega_N) \qquad (12)$$

$$R_2 = (d^2/8)[4J(0) + 3J(\omega_N) + 13J(0.955\omega_H)] + (c^2/6)[4J(0) + 3J(\omega_N)] + R_{ex} \qquad (13)$$

$$\mathrm{NOE} = 1 + (d^2/4R_1)(\gamma_H/\gamma_N)[5J(0.870\omega_H)] \qquad (14)$$

In the simplest case, eqs 12−14 are solved by assuming $J(0.870\omega_H) = J(0.921\omega_H) = J(0.955\omega_H)$; other approximations have been discussed elsewhere (Farrow et al., 1995).

EXPERIMENTAL PROCEDURES

Sample Preparation. A T7*lac* expression vector (Studier & Moffat, 1986) for RNase H was created by subcloning the *rnhA* gene from plasmid pSK58 (gift from W. A. Hendrickson) into the pET-21c plasmid (Novagen). The polymerase chain reaction was used to amplify the *rnhA* gene from pSK58 and introduce *Nde*I and *Hin*dIII restriction sites using chemically synthesized primer sequences (Genosys) 5′-TGGAATTCATATGCTTAAACAGGTAG-3′ and 5′-CCACAAGCTTAAACTTCAACTTGG-3′ (restriction sites are underlined). The amplified product was digested with *Nde*I and *Hin*dIII restriction endonucleases and ligated into the corresponding restriction sites of the pET-21c plasmid. Fidelity of the subcloned *rnhA* gene was confirmed by DNA sequencing (Columbia University Cancer Core Sequencing Facility). The plasmid was used to transform the DL41-

(DE3) *E. coli* strain (gift from W. A. Hendrickson). ^{15}N isotopically enriched *E. coli* RNase H was produced by growing transformed cells at 37 °C in M9 minimal medium containing 1 g/L $^{15}NH_4Cl$ and 40 mg/L ^{15}N-enriched methionine (Cambridge Isotopes) because DL41 is a methionine auxotroph (Hendrickson et al., 1990). Protein expression and purification were performed as described previously (Yang et al., 1990b; Mandel et al., 1995). Typical purified protein yields were 5−10 mg/L of culture.

NMR Spectroscopy. All experiments were performed on a Bruker AMX500 NMR spectrometer operating at a ^1H Larmor frequency of 500.13 MHz and a ^{15}N Larmor frequency of 50.68 MHz. Samples were 1 mM ^{15}N-enriched RNase H in 100 mM $NaCO_2CD_3$ buffer (Isotec) adjusted to pH 5.5 in 90%/10% H_2O/D_2O, 1 mM β-mercaptoethanol, and 2 mM NaN_3. Solvent conditions are identical to those used previously (Mandel et al., 1995), except for the addition of β-mercaptoethanol. Sample temperature was controlled using the spectrometer VT unit; the VT air supply was preconditioned to −20 °C by using a FTS Air-Jet (Model XR-00007-A). The sample temperature was calibrated using a 4% CH_3OH/96% CD_3OD sample and a calibration curve provided by Bruker Instruments. Data sets were processed using Felix 2.30 (MSI) and in-house FORTRAN programs on a Silicon Graphics Indigo workstation or Convex C2 computer. Backbone amide chemical shift assignments at 285 and 310 K were obtained from the assignments at 300 K (Yamazaki et al., 1993; Mandel et al., 1995) by comparing cross-peak resonances from two-dimensional $^1H-^{15}N$ HSQC NMR spectra recorded at 285, 290, 295, 300, 305, and 310 K. Ambiguities in HSQC spectra were resolved by examination of the NH/H^α and NH/H^β cross-peaks in $^1H-^{15}N$ TOCSY-HSQC spectra and sequential $d_{\alpha N}$ and d_{NN} connectivities in $^1H-^{15}N$ NOESY-HSQC spectra recorded at 285 and at 310 K.

Relaxation Measurements. Spin−lattice relaxation rate constants (R_1), spin−spin relaxation rate constants (R_2), and $\{^1H\}-^{15}N$ steady-state heteronuclear Overhauser effects (NOE) for the ^{15}N nuclei in RNase H were measured by two-dimensional sensitivity-enhanced proton-detected heteronuclear NMR spectroscopy using inversion recovery (Vold et al., 1968), CPMG (Carr & Purcell, 1954; Meiboom & Gill, 1958), and steady-state NOE (Noggle & Shirmer, 1971) pulse sequences described previously (Kördel et al., 1992; Skelton et al., 1993). The pulse sequence for the steady-state NOE experiment incorporated the PEP-Z modification to eliminate relaxation differences between the coherence-transfer pathways used to refocus orthogonal magnetization components (Akke et al., 1994). Data were recorded at 285, 300, and 310 K using a single RNase H sample. An additional set of R_1 and NOE measurements were recorded at 300 K using a duplicate sample. All experiments were performed using spectral widths of 2.18 × 12.5 kHz in the $t_1 \times t_2$ dimensions. The ^1H carrier was set to the frequency of the water resonance, and the ^{15}N carrier frequency was set to 115 ppm. Hypercomplex quadrature detection was employed during t_1 evolution periods (Marion et al., 1989b; Akke et al., 1994). The initial values of the t_1 periods were adjusted to 0.5 of the value of the increment to eliminate phase errors and baseline distortions (Zhu et al., 1993). Short (0.5−1.5 ms) spin-lock purge pulses were used for water suppression (Messerle et al., 1989). Decoupling of ^{15}N spins during acquisition was performed using the GARP-1 composite pulse sequence (Shaka et al., 1985) with a radio-frequency field strength of 1.25 kHz (measured as the reciprocal of the 360° pulse length).

Proton decoupling during the relaxation period of R_1 measurements was performed using a train of 180° pulses applied at 4 ms intervals (Boyd et al., 1990). The R_2 measurements were performed with a delay $\tau_{cp} = 1.2$ ms between ^{15}N 180° pulses; proton decoupling was obtained by applying 180° pulses synchronously with even spin echoes during the CPMG pulse train (Kay et al., 1992; Palmer et al., 1992). A recycle delay of 1.5 s was used between transients in the R_1 and R_2 measurements; this delay is approximately three times the spin−lattice relaxation time constant for the amide protons. The R_1 and R_2 measurements were performed using a total of 32 transients per t_1 experiment (including sensitivity enhancement and quadrature detection); 150 × 4096 complex points were acquired in the $t_1 \times t_2$ dimensions. At 285 K, 15 spectra were recorded for the R_1 measurements, using parametric relaxation delays of 0.008 (×2), 0.200, 0.264 (×2), 0.432, 0.640 (×2), 0.920 (×2), 1.33 (×2), 2.11, 3.51 (×2) s (duplicate acquisitions are indicated by the ×2 notation), and 13 spectra were recorded for the R_2 measurements, using relaxation delays of 0.007 (×2), 0.012, 0.022 (×2), 0.031, 0.046 (×2), 0.065, 0.091, 0.137 (×2), 0.274 s. At 300 K, 11 spectra were recorded for the R_1 measurements, using relaxation delays of 0.016 (×2), 0.216 (×2), 0.360, 0.544, 0.800 (×2), 1.22, 2.61 (×2) s, and 15 spectra were recorded for the R_2 measurements, using relaxation delays of 0.007 (×2), 0.022 (×2), 0.036, 0.053 (×2), 0.077, 0.106 (×2), 0.146, 0.214 (×2), 0.461 (×2) s. At 310 K, 13 spectra were recorded for the R_1 experiment, using relaxation delays of 0.016 (×2), 0.032, 0.160 (×2), 0.272, 0.400 (×2), 0.568, 0.824, 1.30, 2.40 (×2) s, and 13 spectra were recorded for the R_2 measurements, using relaxation delays of 0.007 (×2), 0.014, 0.031 (×2), 0.050, 0.074 (×2), 0.108, 0.151, 0.226 (×2), 0.451 s. Relaxation delays at 300 K were identical to those used previously (Mandel et al., 1995).

The NOE was measured from pairs of spectra recorded with and without proton saturation during the recycle delay. Proton saturation during the NOE experiments was obtained by applying a GARP-1 pulse with a field strength of 1.64 kHz for 4 s (Shaka et al., 1985). Control experiments, without proton saturation, used recycle delays of 8 s at 285 K, 12 s at 300 K, and 12 s at 310 K in order to minimize saturation transfer from water protons (Skelton et al., 1993; Li & Montelione, 1994). A continuous wave ^1H radio-frequency field of 1.64 kHz was applied 200 ppm off-resonance for the last 4 s of the recycle delay in the control experiments. The NOE measurements were performed using a total of 64 transients per t_1 experiment; 256 × 4096 complex points were acquired in the $t_1 \times t_2$ dimensions. The NOE measurements were performed in duplicate at each temperature.

Processing of relaxation spectra was done using the same three protocols described previously (Mandel et al., 1995). Briefly, protocol 1, used for well-resolved peaks, maximizes signal to noise by applying an exponential apodization function in the acquisition dimension and a Kaiser function in the indirect dimension (for the NOE experiment, only the first 150 t_1 points were utilized). Protocol 2 enhances resolution by applying a Lorentzian-to-Gaussian transformation in the acquisition dimension. Protocol 3 enhances resolution in both dimensions: a Lorentzian-to-Gaussian

transformation is performed in the acquisition dimension; for R_1 and R_2 data, the t_1 interferogram is extended by a factor of 2 with the HSVD linear prediction algorithm (Barkhuijsen et al., 1987) prior to applying a Kaiser function; resolution in the indirect dimension of the NOE experiment is accomplished by applying a Kaiser function to the full length of 256 t_1 points. A digital low-pass filter was applied to suppress the residual solvent signal (Marion et al., 1989a), data were zero-filled once prior to Fourier transformation, and a fifth-order polynomial baseline correction was applied in the acquisition dimension.

Relaxation parameters were determined from peak heights and uncertainties as described in Mandel et al. (1995). Duplicate spectra were used to determine peak height uncertainties for R_1 and R_2 experiments (Palmer et al., 1991; Skelton et al., 1993) and the standard deviations of the base-plane noise were used to determine peak height uncertainties for NOE experiments. R_1 and R_2 values and uncertainties were determined by nonlinear least squares fitting of the experimental data, and NOE values were determined as the ratios of the peak intensities measured from spectra with and without proton saturation during the recycle delay as described previously (Palmer et al., 1991). Uncertainties in the NOE values were obtained by propagating the uncertainties in the peak heights (Nicholson et al., 1992). NOE experiments were performed twice at each temperature studied; replicate measurements were averaged by using the experimental uncertainties as weighting factors. An additional set of R_1 and NOE measurements were performed on a duplicate RNase H sample at 300 K; the results obtained were averaged by weighting with experimental uncertainties.

Data Analysis. The same five dynamical models utilized previously (Clore et al., 1990a; Mandel et al., 1995) were used to fit the experimental data. These models consist of the following subsets of the extended model-free parameters in eq 4: (1) S^2; (2) S^2, $\tau_e = \tau_f$; (3) S^2, R_{ex}; (4) S^2, $\tau_e = \tau_f$, R_{ex}; and (5) S_f^2, S^2, $\tau_e = \tau_s$, where τ_e refers to the internal time-scale parameter. Model 1 assumes that $S_s^2 = 1$ and $\tau_f \rightarrow 0$. Model 2 is the original formulation of Lipari and Szabo (1982a). Models 3 and 4 are derived from models 1 and 2 by including a nonzero chemical-exchange contribution, R_{ex}. Model 5 is obtained by assuming only that $\tau_f \rightarrow 0$. All models assume a single isotropic rotational correlation time, τ_m. Model-free parameters were determined from the relaxation data by using the in-house FORTRAN program Modelfree (version 3.1) (Palmer et al., 1991). Parsimonious motional models for each bond vector were selected by *F*-statistical testing as described previously (Mandel et al., 1995). The form of the *F*-statistic defined by Mandel et al. (1995) properly accounts for the number of degrees of freedom associated with different models and has greater statistical power than other formulations (Yamasaki et al., 1995b). Statistical properties of the model-free parameters were obtained from Monte Carlo simulations using 300 randomly distributed synthetic data sets (Palmer et al., 1991).

The rotational diffusion anisotropy of RNase H at 285, 300, and 310 K was determined using relaxation rate constants for 37 residues that are located in secondary structural elements, were fit by motional models 1 or 2, and were quantified at all three temperatures. Local diffusion constants, $D_i = (6\tau_{mi})^{-1}$, were determined from the R_2/R_1 ratios (*vide supra*), and the unit vectors, $\mathbf{e}_i$, that define the orientation of the N−H bond vectors were calculated from the atomic coordinates of RNase H in the PDB entry 1RNH with hydrogen atoms built onto the heavy atoms using INSIGHTII (MSI). Equation 11 was solved by least squares optimization for anisotropic, axially symmetric, and isotropic diffusion models. Alternative models were compared using *F*-statistical testing.

Values of the spectral density function at the frequencies $\omega = 0$, ω_N, and $0.870\ \omega_H$ were calculated from the three measured relaxation parameters by inverting eqs 12−14. The value of $J(0.870\omega_H)$ was obtained directly from R_1 and NOE using eq 14. Values of $J(0)$ and $J(\omega_N)$ were obtained by substitution of $J(0.870\omega_H) = J(0.921\omega_H) = J(0.955\ \omega_H)$ into eqs 12 and 13 (Farrow et al., 1995). The apparent value of $J(0)$ obtained by this procedure contains an additional contribution equal to $6R_{ex}/(4d^2 + 3c^2)$ from chemical exchange. Uncertainties were obtained by error propagation.

RESULTS

RNase H has 149 backbone amide groups expected to give resonance signals in $^1H-^{15}N$ HSQC spectra; however, weak or overlapping resonances are difficult to quantitate for spin relaxation measurements. At 285 K, 121 of the expected 149 residues were studied. Of these, 70 were quantified using protocol 1 (exponential line-broadening apodization in ω_2), 34 using protocol 2 (Lorentzian-to-Gaussian transformation in ω_2), and 17 using protocol 3 (resolution enhancement in ω_1 and Lorentzian-to-Gaussian transformation in ω_2). At 300 K, 124 residues were studied: 66 were quantified with protocol 1, 34 with protocol 2, and 24 with protocol 3. At 310 K, 123 residues were studied: 96 were quantified using protocol 1, 12 using protocol 2, and 15 using protocol 3. Broadening of the peaks at 285 K due to an increase in the global tumbling time (*vide infra*) reduced signal-to-noise ratios and increased resonance overlap, thus rendering quantification more difficult at this temperature. A greater number of residues were quantified at 300 K compared with the previous study (118 residues) (Mandel et al., 1995). In total, 109 residues were quantitated at all three temperatures, 116 residues were quantitated at both 285 and 300 K, 112 residues were quantitated at both 285 and 310 K, and 117, residues were quantitated at both 300 and 310 K. Residues Glu 32, Ile 53, and Glu 64 could be quantified only at 285 K; residues Asn 16 and His 124 could be quantified only at 300 K; and residues Gln 4, Gln 76, Trp 85, and Ala 137 could be quantified only at 310 K.

The relaxation data for all three temperatures are given in the Supporting Information. The 10% trimmed weighted mean results at 285, 300, and 310 K were respectively 1.132 ± 0.004, 1.578 ± 0.002, and 1.868 ± 0.002 s^{-1} for R_1; 16.42 ± 0.05, 10.84 ± 0.02, and 8.99 ± 0.01 s^{-1} for R_2; and 0.722 ± 0.007, 0.741 ± 0.005, and 0.736 ± 0.002 for NOE. The 10% trimmed weighted average value of the R_2/R_1 ratio was 14.53 ± 0.06 at 285 K, 6.86 ± 0.01 at 300 K, and 4.81 ± 0.01 at 310 K. In general, the data taken at 285 K had 2−4-fold less precision than at 300 or 310 K, reflecting the lower signal to noise at 285 K due to increased line widths. The mean results at 300 K differ slightly from the corresponding results of 1.502 ± 0.003 s^{-1} for R_1, 11.28 ± 0.03 s^{-1} for R_2, and 0.812 ± 0.008 for NOE reported in Mandel et al. (1995). The difference in the NOE result is a consequence of the 2−3-fold longer recycle delays used in the NOE experiments in the present study (minimizing saturation transfer effects).

Relaxation data were fit by motional models 1 through 5, respectively, for 64, 12, 30, 0, and 15 ^{15}N spins at 285 K;

55, 10, 40, 1, and 18 spins at 300 K; and 49, 17, 39, 4, and 14 spins at 310 K. Model selection at 300 K in Mandel et al. (1995) yielded 67, 9, 29, 2, and 9 spins for models 1 through 5, respectively. Quality of the model selection and fitting was assessed by examining the residual sum square error for each spin. For model 1, the $\alpha = 0.05$ critical value is ~6.0; for models 2 and 3, the $\alpha = 0.05$ critical value is ~3.8; and for models 4 and 5, the residual sum square error is required to be 0. At 285 K, 109 of the 121 nuclear spins had residual sum square errors less than the $\alpha = 0.05$ critical values (or zero for models 4 and 5), 4 had residual sum square errors slightly larger than the $\alpha = 0.05$ critical values, and 8 had residual sum square errors in the range 9−15. At 300 K, 110 of the 124 nuclear spins had residual sum square errors less than the $\alpha = 0.05$ critical values (or zero for models 4 and 5), 9 had residual sum square errors slightly larger than the $\alpha = 0.05$ critical values, and 5 had residual sum square errors in the range 11−18. At 310 K, 95 of the 123 nuclear spins had residual sum square errors less than the $\alpha = 0.05$ critical values (or zero for models 4 and 5), 15 had residual sum square errors slightly larger than the $\alpha = 0.05$ critical values, and 13 had residual sum square errors in the range 9−20.

The model selection strategy yielded the same motional model at 285, 300, and 310 K for 71 of the 109 residues that were quantified at all three temperatures. Most differences in motional models for the other 38 residues involved the addition or removal of one parameter at either 285 or 310 K relative to 300 K. In addition, Arg 27, Arg 46, Arg 75, Ala 93, Trp 120, Ala 141, and Asn 143 were fit with the same model at 285 K and at 310 K, but with the addition or removal of one parameter at 300 K. Two residues, Gly 20 and His 114, show larger discrepancies between temperatures. Gly 20 is fit with model 5 at 300 K and with model 1 at both 285 and 310 K. Gly 20, in general, is anomalous, in that the sum squared error at 310 K is large (12.43) and also that a substantial number of Monte Carlo simulations (191/300) do not converge at 300 K. His 114 is fit with three different models: model 1 at 285 K, model 3 at 300 K, and model 4 at 310 K. Residues Met 47 and Ile 53, located in α_A, gave elevated, but acceptable, residual sum square errors for model 1 at 285 K but were fit with model 3 at 300 and 310 K. In order to determine the temperature dependence of R_{ex} terms for residues in α_A and α_D (*vide infra*), model 3 was used to analyze the data for Met 47 and Ile 53 at all three temperatures. When model 3 is used instead of model 1, the order parameters change at 285 K from 0.982 ± 0.027 to 0.927 ± 0.044 for Met 47 and from 0.906 ± 0.031 to 0.828 ± 0.046 for Ile 53.

After final optimization with the selected dynamical model for each nuclear spin, the global value of τ_m was 14.38 ± 0.04 ns at 285 K, 9.28 ± 0.02 ns at 300 K, and 7.36 ± 0.01 ns at 310 K. The value of τ_m at 300 K agrees with the previously determined value of 9.69 ± 0.02 ns (Mandel et al., 1995) to within 4.4%. For a spherically symmetric molecule, $\tau_m = V\eta/(k_B T)$, in which V is the hydrated volume of the molecule and η is the viscosity of the solution. A least squares fit yields $V = (4.54 \pm 0.03) \times 10^{-20}$ cm^3 (r = 0.981) and a hydrated radius of 22.1 ± 0.1 Å. Hydrodynamic calculations using the program HYDRO (Garcia de la Torre & Bloomfield, 1981) with stick boundary conditions (Cantor & Schimmel, 1980) indicate that ~125 waters of hydration are required to reproduce the experimental rotational diffusion coefficients (L. K. Lee and A. G. Palmer, unpublished results). Analysis of the R_2/R_1 ratios using the local diffusion approach indicates that the rotational diffusion tensor for RNase H is axially symmetric with $D_\parallel/D_\perp = 1.12 \pm 0.02$; the unique axis in the diffusion tensor frame is oriented with $\theta = 82 \pm 4°$ and $\phi = 152 \pm 3°$ relative to the molecular frame of the PDB coordinate file 1RNH. Possible effects of rotational diffusion anisotropy on the present results are discussed below.

Numerical values of the model-free motional parameters at all three temperatures are given in Supporting Information and are depicted graphically in Figure 3. Mean order parameters for secondary structural elements are given in Table 1. The order parameters and the chemical-exchange rate constants are mapped onto the structure of RNase H in Figure 4. While the overall pattern of order parameters is similar at all three temperatures, the weighted mean order parameter for secondary structure elements of 0.879 ± 0.002 at 285 K, 0.853 ± 0.001 at 300 K, and 0.851 ± 0.001 at 310 K displays a slight decrease with increasing temperature. Temperature dependence of the order parameters for selected structural elements is shown in greater detail in Figure 5.

A graph of $1 - S$ versus T is illustrated in Figure 6a for secondary structural elements, for residue Gly 126 in the loop between β_5 and α_E, and for residue Gln 152 at the C-terminus. Values of $d(1 - S)/dT$ for the 71 residues quantified with the same motional model at all three temperatures are given in Figure 6b. The slope of the least squares lines yields an average $d(1 - S)/dT = (4.1 \pm 0.6) \times 10^{-4}$ K^{-1} for secondary structural elements. A slight systematic anti-correlation is observed between the temperature dependence of chemical-exchange and the order parameters (*vide infra*); this effect is seen most clearly for residues in α_D, in which $d(1 - S)/dT$ is negative. If residues fit with chemical-exchange terms (models 3 and 4) are excluded, then the average $d(1 - S)/dT = (5.9 \pm 0.7) \times 10^{-4}$ K^{-1} for secondary structural elements. The C-terminal and loop regions display a slightly greater temperature dependence than secondary structure elements: the average values of $d(1 - S)/dT$ are $(1.6 \pm 0.2) \times 10^{-3}$ K^{-1} for Lys 91, Thr 92, and Lys 95 in the handle region; $(2.1 \pm 0.3) \times 10^{-3}$ K^{-1} for residues Gly 123, Ala 125, Gly 126, and His 127 in the loop between β_5 and α_E; and $(3.6 \pm 0.1) \times 10^{-3}$ K^{-1} for residues Gln 152, Glu 154, and Val 155 at the C-terminus.

The effective internal correlation times for both fast (model 2 and model 4) and slow (model 5) time scales are independent of temperature within experimental uncertainties. Phenomenological Arrhenius plots of $\ln\tau_e$ versus $1/T$ (not shown) indicate that activation energies less than ~10 kJ/mol cannot be distinguished statistically from zero for residues fit with model 2 ($\tau_e = \tau_f$), and activation energies less than ~5 kJ/mol cannot be distinguished from zero for residues fit with model 5 ($\tau_e = \tau_s$).

Figure 3 shows that the magnitudes of the R_{ex} terms generally decrease with increasing temperature for residues fit with models 3 and 4. Thus, the exchange rate must satisfy $k_{ex} > 3.2/\tau_{cp} = 2.7 \times 10^3$ s^{-1}. Most residues in α_A and α_D are fit with model 3 to account for chemical-exchange broadening due to motions on the microsecond to millisecond time scale. For the nine residues in α_A fit with model 3 at all three temperatures, the weighted mean values of R_{ex} are 2.55 ± 0.26 s^{-1} at 285 K, 1.47 ± 0.09 s^{-1} at 300 K, and 1.01 ± 0.05 s^{-1} at 310 K. For the eight residues in α_D studied at all three temperatures, the weighted mean values

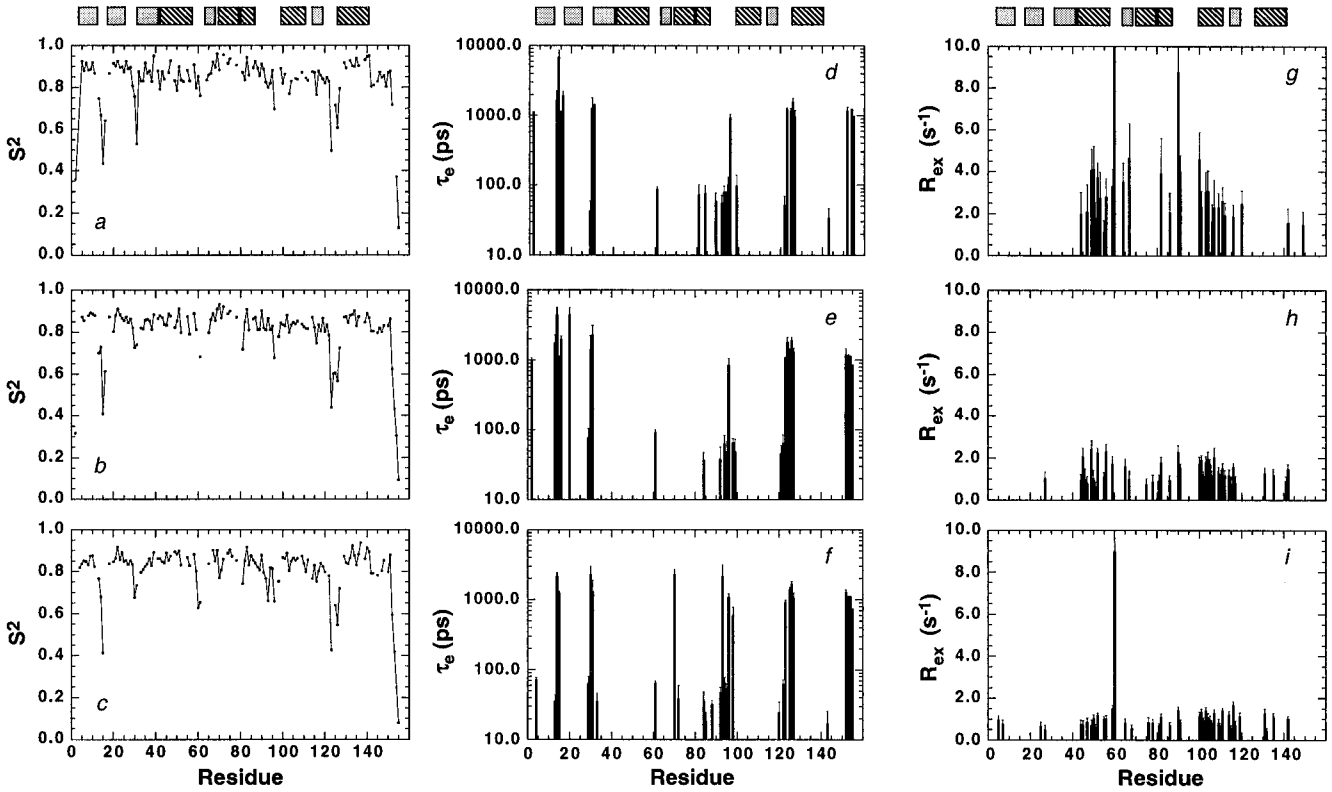

FIGURE 3: Dynamical parameters for *E. coli* RNase H. Order parameters, S^2, are plotted versus residue number at (a) 285 K, (b) 300 K, and (c) 310 K; internal correlation times, τ_e, are plotted versus residue number at (d) 285 K, (e) 300 K, and (f) 310 K; and phenomenological CPMG chemical exchange rate constants, R_{ex}, are plotted versus residue number at (g) 285 K, (h) 300 K, and (i) 310 K. At 285 K, the value of R_{ex} for Lys 60 is 23 ± 4. At 300 K, the resonance for Lys 60 is overlapped with the resonance for Ile 7 and cannot be quantified. Error bars are not shown for (a)−(c) for clarity; average uncertainties in S^2 are 0.024, 0.011, and 0.010 for 285, 300, and 310 K, respectively. Dark rectangles represent β-sheet regions and hatched rectangles represent α-helical regions of RNase H.

Table 1: Order Parameters for Secondary Structural Elements

		$\langle S^2 \rangle^b$		
2nd str[a]	sequence[a]	285 K	300 K	310 K
β_1	4−13	0.869 ± 0.008 (8)	0.863 ± 0.004 (7)	0.830 ± 0.003 (9)
β_2	18−27	0.900 ± 0.008 (9)	0.874 ± 0.003 (9)	0.866 ± 0.003 (9)
β_3	32−42	0.861 ± 0.006 (10)	0.848 ± 0.002 (9)	0.838 ± 0.002 (9)
α_A	43−59	0.868 ± 0.008 (13)	0.856 ± 0.003 (13)	0.860 ± 0.002 (13)
β_4	64−69	0.895 ± 0.011 (6)	0.864 ± 0.004 (5)	0.881 ± 0.005 (4)
α_B	71−80	0.932 ± 0.014 (4)	0.893 ± 0.005 (5)	0.867 ± 0.004 (6)
α_C	81−88	0.900 ± 0.008 (7)	0.856 ± 0.003 (7)	0.842 ± 0.002 (8)
α_D	100−112	0.840 ± 0.010 (9)	0.835 ± 0.002 (12)	0.849 ± 0.003 (12)
β_5	115−120	0.838 ± 0.009 (6)	0.806 ± 0.004 (6)	0.807 ± 0.004 (6)
α_E	127−142	0.905 ± 0.006 (12)	0.865 ± 0.002 (13)	0.872 ± 0.002 (14)

[a] Secondary structure designations are from Yang et al. (1990a). [b] Weighted mean order parameter and standard error in the mean, calculated from the data in Table S2. The number of residues averaged for each entry is given in parentheses.

of R_{ex} are 2.55 ± 0.30 s^{-1} at 285 K, 1.61 ± 0.087 s^{-1} at 300 K, and 1.20 ± 0.05 s^{-1} at 310 K. Residues Ile 82 and Lys 86 in α_C and Trp 90 and Lys 91 in the handle region also were fit with model 3 at all three temperatures. Arrhenius plots of $\ln R_{ex}$ versus $1/T$, shown in Figure 7, were used to determine an apparent activation energy, E_a, for each residue undergoing exchange. The activation barriers are presented in Table 2. The weighted mean activation barriers are 33 ± 3 kJ/mol for α_A and 23 ± 3 kJ/mol for α_D.

Figure 8 presents the difference between the order parameters and chemical-exchange terms obtained in the present study and the results reported previously by Mandel et al. (1995). Of the 113 residues quantitated in both studies, 77 were fit with the same motional model. Nine residues, Leu 2, Cys 13, Leu 14, Gly 20, Gly 30, Gly 123, Ala 125, Gly 126, and His 127, located in loops or termini, were fit with model 1 or 2 in the original data but model 5 in the present data. Differences for six residues involved addition or subtraction of $\tau_e = \tau_f$ as a parameter. The present mean secondary structure order parameter of 0.853 ± 0.001 at 300 K agrees well with the value of 0.854 ± 0.002 reported previously by Mandel et al. (1995). The weighted mean difference (± sample deviation) between the new and original data sets for 113 residues (including loops and termini) is −0.012 ± 0.016. The *t*-statistic for the differences in order parameters between two data sets is defined as $t = (S_2^2 - S_1^2)(\sigma_2^2 + \sigma_1^2)^{-1/2}$ with one degree of freedom, in which σ_1 and σ_2 are the sample deviations. A similar expression can be written for R_{ex}. A two-tailed *t*-test indicates that 11 residues (Cys 13, Gly 30, Glu 61, Ser 71, Trp 81, Ala 125, Arg 132, Asp 134, Val 153, Glu 154, and Val 155) differ significantly at a confidence level $\alpha = 0.20$ ($t = 3.08$) and 2 residues (Asp 134 and Val 155) differ significantly at a confidence level $\alpha = 0.10$ ($t = 6.31$). Eleven residues were

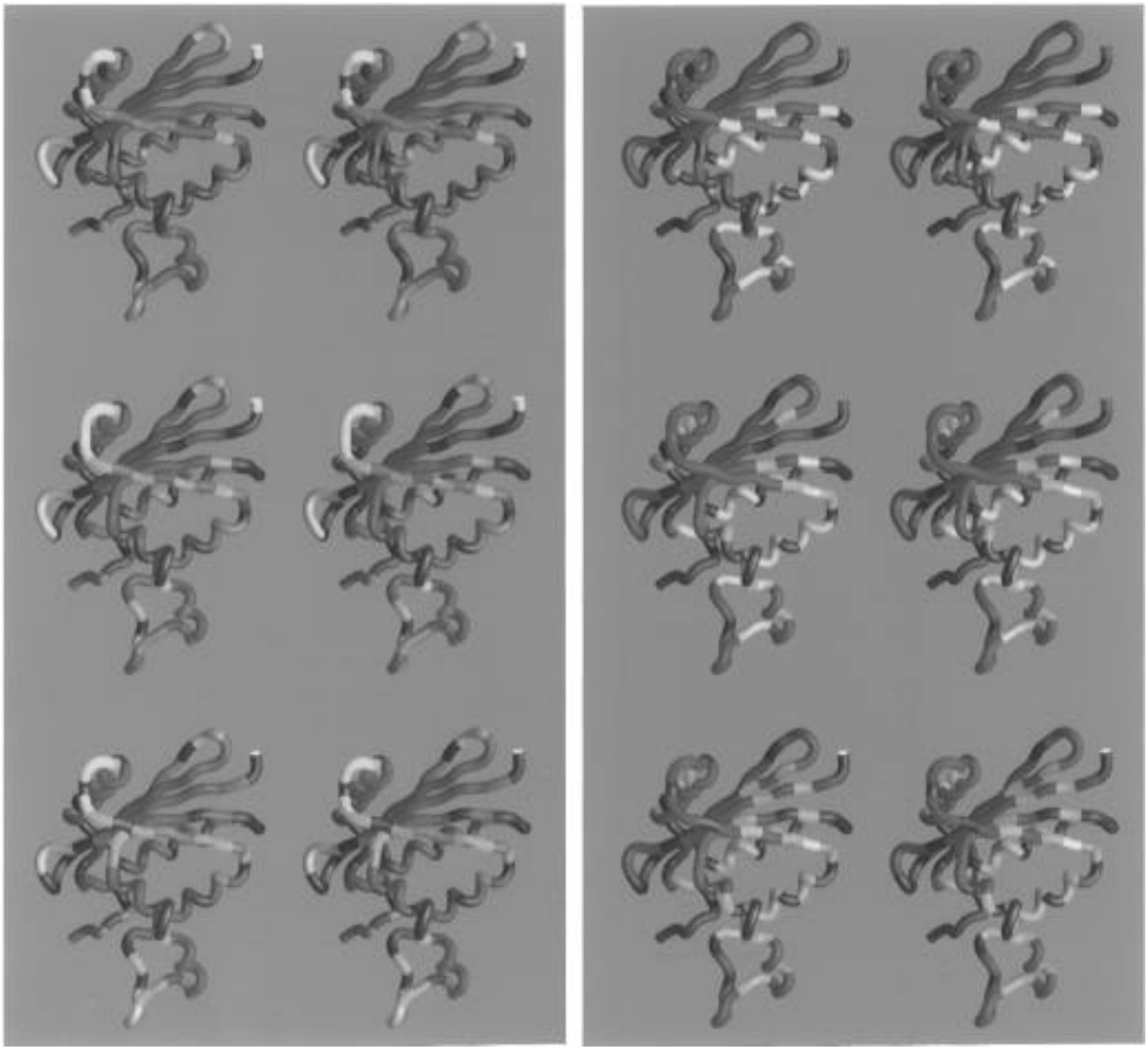

FIGURE 4: Stereoviews of the backbone C^{α} chain trace of *E. coli* RNase H. (Left) The structure is color-coded by the value of the generalized order parameters at (top) 285 K, (middle) 300 K, and (bottom) 310 K. The color scheme is blue, $S^2 \geq 0.85$; and yellow, $S^2 \leq 0.60$. Colors are interpolated continuously for intermediate values of S^2. (Right) The structure is color-coded by the value of the chemical-exchange terms, R_{ex}, at (top) 285 K, (middle) 300 K, and (bottom) 310 K. The color scheme is blue, $R_{ex} = 0.0\ s^{-1}$; and yellow, $R_{ex} \geq 2.0\ s^{-1}$. Colors are interpolated continuously for intermediate values of R_{ex}. Residues for which motional parameters were not determined are colored charcoal. The structure coordinates were obtained from the PDB entry 1RNH (Yang et al., 1990a). Four C-terminal residues not observed crystallographically were built onto the structure in an extended conformation using INSIGHTII (MSI). The figure was prepared using GRASP (Nicholls et al., 1991).

fit with R_{ex} in the present data but not in the original data; ten residues were fit with R_{ex} in the original data but not in the present data. The majority of these residues had R_{ex} terms less that 1 s^{-1}. For 22 residues fit with models 3 or 4 in both data sets, the weighted mean difference ($\pm$ sample deviation) between the new and original data is -0.30 ± 0.48. Met 142 ($t = 2.8$) was the only residue with a *t*-statistic greater than 2.0.

Values of the spectral density function, $J(0)$, $J(\omega_N)$, and $J(0.87\omega_H)$, at 285, 300, and 310 K, derived using the reduced spectral density mapping procedure (eqs 12−14), are given in Figure 9. Values of $J(0)$ decrease with increasing temperature due to the decreased rotational correlation time at higher temperatures. As a consequence of the normalization of $J(\omega)$, the values of the higher frequency terms, $J(\omega_N)$ and $J(0.87\omega_H)$, necessarily increase with increasing temperature. Because $\tau_m \gg \tau_e$, $J(0) \approx S^2\tau_m + 6R_{ex}/(4d^2 + 3c^2)$ and, in the absence of chemical exchange, $J(0)$ is a linear function of S^2 with slope τ_m. Consequently, as shown in Figure 9d, the slope of a plot of $J(0)$ versus S^2 decreases as the temperature is increased, and chemical-exchange increases $J(0)$ above the canonical line. Because $(\omega_H\tau_m)^2 \gg 1$, $J(0.87\omega_H) \approx (1 - S^2)\tau_e/[1 + (\omega_H\tau_e)^2]$. At a magnetic field strength of 11.74 T, dynamic processes with $\tau_f < 100$ ps and processes with $\tau_s \approx 1$ ns coincidentally generate similar values for $J(0.87\omega_H)$. Consequently, a linear dependence between $J(0.87\omega_H)$ and S^2 is observed in Figure 9f, in which $J(0.87\omega_H)$ is increased for residues with significant conformational dynamics on picosecond to nanosecond time scales. Terms proportional to S^2 and to $1 - S^2$ in the spectral density function become comparable for $J(\omega_N)$ if $\tau_e = \tau_s = 1$ ns and simple linear dependence between $J(\omega_N)$ and S^2 is not obtained for those residues fit with model 5 in the model-free analysis.

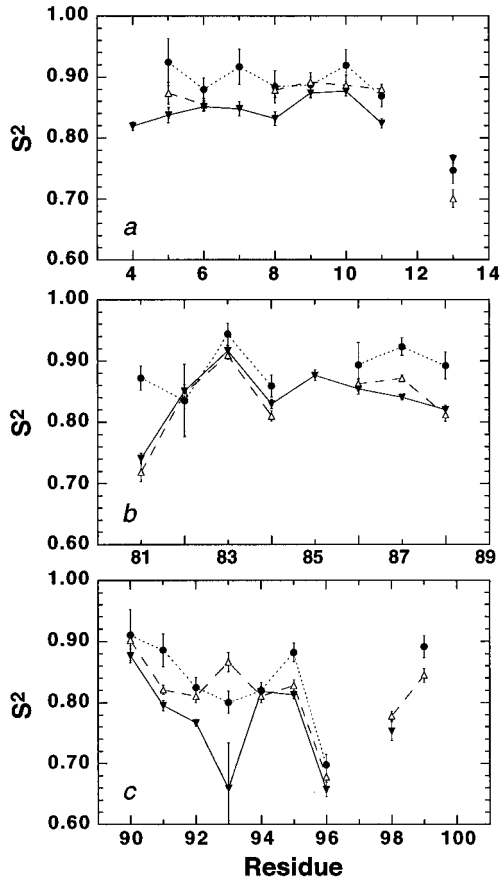

FIGURE 5: Temperature dependence of order parameters for selected structural elements in *E. coli* RNase H. Shown are (a) β_1, (b) α_C, and (c) the handle region for temperatures of (●) 285 K, (△) 300 K, and (▼) 310 K.

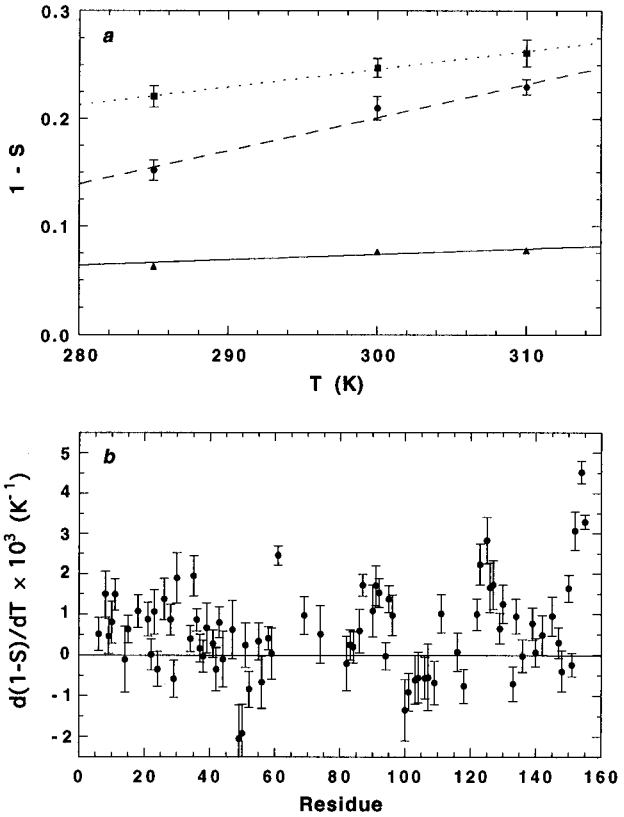

FIGURE 6: Temperature dependence of order parameters. (a) Shown are $1 - S$ versus T for (▲) the average value for secondary structural elements, (■) Gly 125, and (●) Gln 152. Error bars for the secondary structure elements are smaller than the plotted symbols. (b) Shown are values of $d(1 - S)/dT$ versus residue number for residues that were quantitated with the same motional model at 285, 300, and 310 K.

DISCUSSION

Comparison with Previous Results. Despite the fairly large number of backbone ^{15}N spin relaxation studies of proteins that have been reported in the literature (Palmer, 1993; Wagner, 1993), the reproducibility of the experimental results has not been tested directly. Independent data sets now have been reported for RNase H at 300 K by Mandel et al. (1995), by Yamasaki et al. (1995), and in the present study. These three data sets present the first opportunity to evaluate reproducibility within and between laboratories. A quantitative comparison of experimental and computational results will be presented elsewhere (Philippopoulos et al., 1996); herein, the major conclusions derived from the comparison between the present data and the previous data reported by Mandel et al. (1995) are summarized.

As presented above, order parameters for 111 of the 113 residues quantified in both data sets agree within experimental uncertainties at the $\alpha = 0.10$ confidence level and 102 agree at the $\alpha = 0.20$ confidence level. The between-sample reproducibility of $0.016/2^{1/2} = 0.011$ is similar to the uncertainties derived from the error analyses performed for each data set individually, as part of the model-free analysis. This result suggests that experimental uncertainties are being evaluated appropriately during data analysis. Three regions of the protein contain residues with consistently large absolute deviations (but large uncertainties) between the two data sets: the loop between β_1 and β_2, the loop between β_5 and α_E, and residues Asp 10 and Ser 71 in the active site. The loop between β_1 and β_2 contains three residues, Cys 13 ($t = -3.54$), Leu 14 ($t = -2.60$), and Gly 15 ($t = -2.03$), that have lower order parameters in the present data set. The loop between β_5 and α_E displays enhanced mobility in both studies, but residues Lys 122 ($t = -1.50$), Gly 123 ($t = -1.38$), Ala 125 ($t = -4.34$), Gly 126 ($t = -1.94$), and His 127 ($t = -1.43$) have lower order parameters in the present study. These residues were fit with models 1 or 2 in Mandel et al. (1995) and with model 5 herein. Asp 10 ($t = 1.20$) and Ser 71 ($t = 3.22$) have higher order parameters in the present data set. In addition, a large chemical-exchange term with high uncertainty (4.6 ± 1.4 s^{-1}) was obtained for Ser 71 in Mandel et al. (1995), but no chemical-exchange terms were observed in the present data. The resonance signal from the conserved active site residue Glu 70 was too weak and broad in the initial study to be quantitated; in the present study, this residue reports an order parameter of 0.932 ± 0.016. All of these residues are either active site residues or are located in loops considered important for substrate binding. These residues have very weak amide resonance signals in the original data set (generally yielding model-free parameters with high uncertainties) and substantially sharper and more intense signals in the new data set (generally yielding model-free parameters with low uncertainties). One hypothesis consistent with these observations is that the active site residues and residues in loops surrounding the active site were exchange broadened in the original sample of RNase H by reversible binding of a small ionic or molecular species.

In the experimental protocol utilized herein, chemical exchange is recognized as a systematic increase in R_2 over values predicted for dipolar and chemical shift anisotropy relaxation measurements. Consequently, the accuracy of R_{ex}

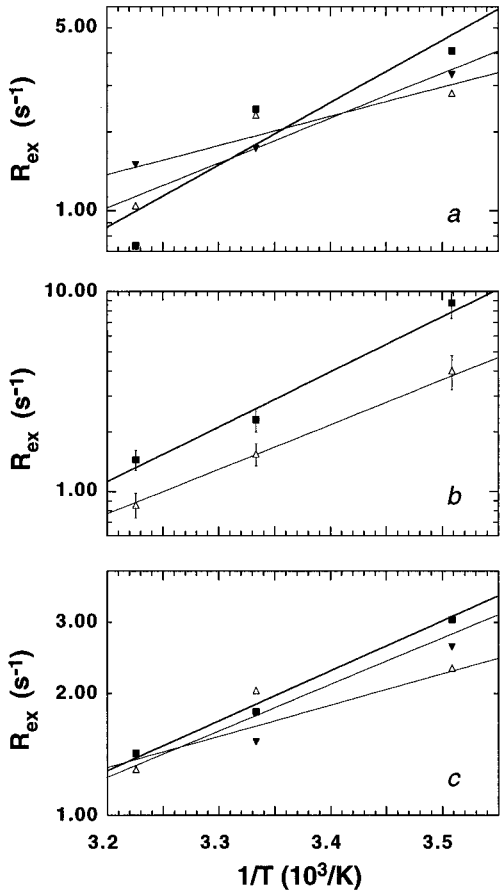

FIGURE 7: Temperature dependence of chemical exchange for selected structural elements in *E. coli* RNase H. Shown are Arrhenius plots of lnR_{ex} versus $1/T$ for (a) residues (■) Leu 49, (△) Leu 56, and (▼) Leu 59 in α_A; (b) residues (■) Trp 90 and (△) Lys 91 in the handle region; and (c) (■) Leu 103, (△) Leu 107, and (▼) Leu 111 in α_D. Apparent activation energies derived from the slope of the graphs are given in Table 2. For clarity, error bars are only shown for (b).

values has long been of concern, and in particular, control calculations have been utilized to ascertain whether values of the order parameters and chemical-exchange terms were correlated during the numerical analysis of relaxation data (Mandel et al., 1995). The present data provide the first direct evidence for the reproducibility of chemical-exchange terms. Three conclusions are evident from the comparison between the present and original data at 300 K. (1) Small values of $R_{ex} < 0.5$ s^{-1} are not robustly identified by the model selection protocol and should be interpreted with caution. (2) The statistical reproducibility of R_{ex} terms that are consistently identified by the model selection protocol is 0.48 s$^{-1}/2^{1/2} = 0.34$ s^{-1} and is similar to the statistical uncertainty measured from individual data sets; most of these residues have $R_{ex} > 1.0$ s^{-1} and can be interpreted with confidence. (3) R_{ex} and S^2 are slightly anticorrelated by the numerical analysis; thus, order parameters are somewhat artifactually reduced for residues exhibiting large R_{ex} values. Assuming that the true value of $d(1 - S)/dT$ for α_A and α_D is equal to the average value for other secondary structures in the absence of exchange, then the value of S^2 is reduced by $(0.018 \pm 0.004)R_{ex}$.

RNase H has an axially symmetric diffusion tensor with $D_{||}/D_{\perp} = 1.12$; thus, the values of R_2 for residues with N−H vectors preferentially oriented along the direction defined by $D_{||}$ are potentially increased by as much as ∼6% compared with the result for an isotropic sphere. The data analysis

Table 2: Apparent Activation Energies for Chemical Exchange

residue[a]	2nd str[b]	E_a (kJ/mol)[c]	$\chi^{2\,d}$
Asn 44	α_A	25 ± 17	0.2
Met 47	α_A	14 ± 23	0.7
Leu 49	α_A	46 ± 9	4.4
Met 50	α_A	37 ± 10	2.4
Ala 51	α_A	26 ± 16	0.9
Ala 52	α_A	36 ± 5	2.8
Ala 55	α_A	8 ± 11	0.1
Leu 56	α_A	33 ± 8	3.8
Leu 59	α_A	21 ± 8	0.5
Ile 82	α_C	38 ± 10	4.6
Lys 86	α_C	28 ± 14	0.1
Trp 90	handle	52 ± 6	1.9
Lys 91	handle	43 ± 7	0.1
Asn 100	α_D	41 ± 11	0.2
Val 101	α_D	20 ± 7	0.8
Leu 103	α_D	24 ± 8	0.1
Trp 104	α_D	32 ± 9	0.7
Arg 106	α_D	22 ± 12	0.2
Leu 107	α_D	22 ± 12	0.5
Ala 109	α_D	30 ± 10	0.2
Leu 111	α_D	6 ± 8	0.7

[a] Residue number for residues in α_A, α_C, α_D, and the handle region exhibiting significant chemical exchange at 285, 300, and 310 K. [b] Secondary structure designations are from Yang et al. (1990a). [c] Apparent activation energy derived from least squares fits to the Arrhenius equation as shown in Figure 7. [d] χ^2 statistic from least squares fit. A value less than 3.8 indicates a satisfactory fit at the $\alpha = 0.05$ confidence level.

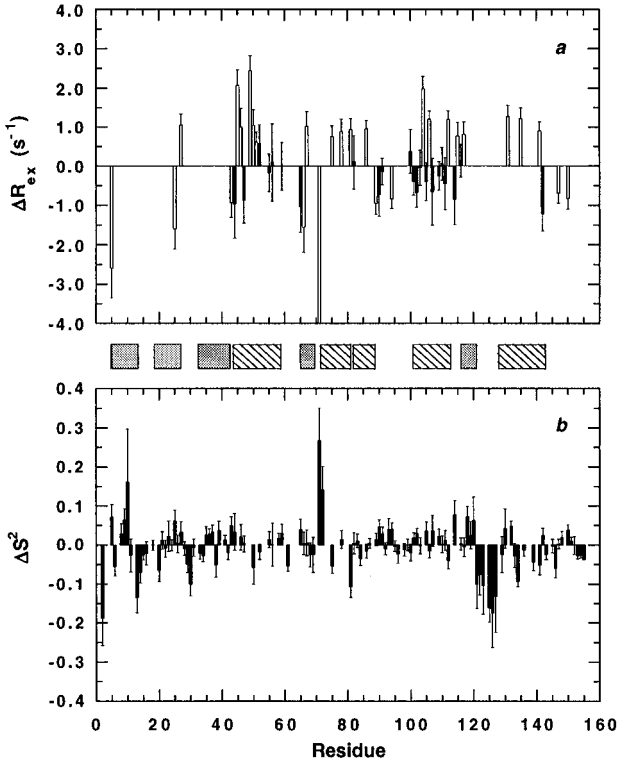

FIGURE 8: Comparison of (a) order parameters and (b) chemical-exchange terms for independent data sets. Shown are the differences between the present data for 300 K and data from Mandel et al. (1995). In (a) residues for which R_{ex} was fitted in both data sets are indicated by dark bars; residues for which R_{ex} was fitted in only one data set are indicated by hollow bars.

protocol can introduce artifactual R_{ex} terms to compensate for the effect of anisotropic diffusion. For RNase H at 285, 300, and 310 K, values of R_{ex} less than 1, 0.6, and 0.5 s^{-1}, respectively, may arise from anisotropic diffusion rather than actual chemical exchange. The principal conclusions derived from the temperature dependence of conformational ex-

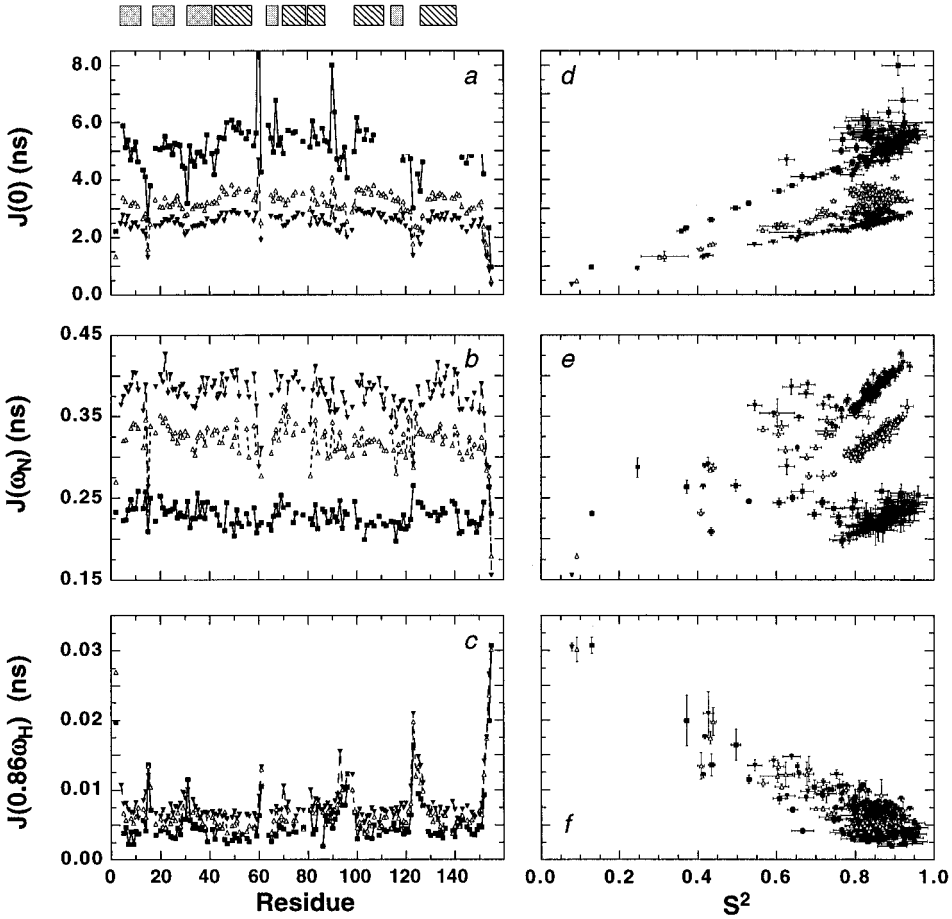

FIGURE 9: Reduced spectral densities for *E. coli* RNase H. Values of (a) $J(0)$, (b) $J(\omega_N)$, and (c) $J(0.87\omega_H)$ are plotted versus residue number; values of (d) $J(0)$, (e) $J(\omega_N)$, and (f) $J(0.87\omega_H)$ are plotted versus the generalized order parameter, S^2. Within each graph, data are shown for (■) 285 K, (△) 300K, and (▼) 310 K. Error bars are not shown in (a)−(c) for clarity.

change are not altered by consideration of rotational anisotropy of this magnitude.

Temperature Dependence of Order Parameters. The decrease in order parameters and the invariance of internal effective correlation times observed at higher temperatures in the present study are consistent with increased amplitudes of motion of the N−H bond vectors within a single conformational minimum or within a set of conformational minima separated by low energetic barriers. Generally, the magnitude of the temperature dependence of the order parameters varies with C-terminus > loops > secondary structure. The cone semiangle associated with each order parameter by the diffusion-in-a-cone motional model indicates that the angular conformational space accessible to N−H bond vectors increases by ∼2° for secondary structural elements and ∼5° for the C-terminus over the temperature range from 285 to 310 K. The characteristic temperature parametrizes the distribution of thermally accessible conformational states. If $T^*/T \gg 1$, then few additional states are populated upon an increase in temperature; in contrast, if $T^*/T \leq 1$, then many states are accessible upon an increase in temperature. The average temperature dependence $d(1 - S)/dT$ of the order parameters yields characteristic temperatures ranging from ∼170 K for the C-terminus to ∼1000 K for secondary structure elements. Thus, at 300 K, $T^*/T \approx 3$ for the secondary structure elements, $T^*/T \approx 1$ for residues in the handle and in the loop between β_5 and α_E, and $T^*/T \approx 0.6$ for the C-terminus. These results suggest that intramolecular dynamics in RNase H are manifestations of a hierarchy of energy states, or so-called "conformational substates" (Frauenfelder et al., 1988), thermally accessible to the ^{15}N bond vectors. In particular, the results for secondary structure elements indicate that the energy scale governing the conformational distribution of bond vector orientations is $\sim 3k_BT$, as compared with the free energy of unfolding of $\sim 20k_BT$ for *E. coli* RNase H (Chamberlain et al., 1996). Thus, the conformational dynamics of backbone N−H bond vectors in secondary structure elements are coupled to structural perturbations yielding relatively high energy local intermediate states; in contrast, loop and termini dynamics do not necessitate transitions to significantly higher energy states. The characteristic temperature also is closely connected to the heat capacity of a conformational mode. If $T^*/T \gg 1$, then the mode has low heat capacity because few states are thermally accessible; in contrast, if $T^*/T \leq 1$, then the heat capacity is given by the classical limit of $\sim k_B$ because many conformational states are thermally accessible. A second conclusion of the present results is that the conformational dynamics of the secondary structure contribute little to the heat capacity of the folded state of RNase H and consequently may provide a significant contribution to the difference in heat capacity between folded and unfolded states.

The loop between β_1 and β_2, the loop between β_5 and α_E, and the handle region surround the active site in RNase H. These regions contain residues with reduced order parameters at all three temperatures studied (Leu 14 to Asn 16 for the loop between β_1 and β_2; Gly 123 to His 127 for the loop between β_5 and α_E; and Lys 96 and Val 98 in the handle region). The values of $d(1 - S)/dT$ are ∼3−4-fold larger

for residues in these loops than for secondary structure elements. Changes in order parameters upon ligand binding can be related theoretically to changes in free energy and conformational entropy (Akke et al., 1993; Yang & Kay, 1996). Consequently, the temperature dependence of the flexibility of these loops may contribute to the temperature dependence of binding affinity in RNase H.

The temperature dependence of the order parameters of amide nuclei located in β_5, which is located at one edge of the five-stranded β-sheet, is particularly noteworthy. At 285 K, the order parameters are relatively large and uniform, except for Ile 116. At 300 K, the order parameters alternate between high and low values with low values observed for amide groups hydrogen bonded to solvent rather than to β_4. At 310 K, the experimental data for Trp 118 are not well fit; for other residues, the order parameters are reduced even for residues hydrogen bonded to β_4. The overall patterns suggest that β_5 is progressively thermally destabilized relative to the rest of the β-sheet and that destabilization occurs initially for residues hydrogen bonded to solvent followed by residues hydrogen bonded to the adjacent β-strand, β_4.

Temperature Dependence of Effective Correlation Times. The present data are insufficient to determine apparent activation energies less than ~10 kJ/mol for effective correlation times <100 ps (motional models 2 and 4) and less than ~5 kJ/mol for effective correlation times of ~1 ns (motional model 5). Higher precision and a wider temperature range would be required to detect smaller activation energies. Nonetheless, the result that the activation barriers for motions on the picosecond to nanosecond time scale are less than 5−10 kJ/mol restricts the allowable mechanisms for these conformational processes. For example, dynamic mechanisms that posit breaking of multiple hydrogen bonds are incommensurate with the experimental results, unless bond breaking and formation are concerted. Although motional parameters derived for model 5 have zero degrees of statistical freedom, and consequently may be less accurate than motional parameters derived from other models, the congruence between the results at different temperatures supports the reliability of the analysis for RNase H.

Temperature Dependence of Chemical Exchange. A striking aspect of the present results is the preponderance of thermally activated conformational exchange processes in RNase H, particularly in α_A, α_C, α_D, and the handle region. These structural elements form a contiguous region that includes much of the hydrophobic core of RNase H. The pronounced temperature dependence of the motions in α_A and α_D is noteworthy particularly in light of investigations of protein folding and stability of RNase H that identify these two helices as forming the structural core of the molecule (Dabora & Marqusee, 1994; Yamasaki et al., 1995a; Chamberlain et al., 1996). The chemical-exchange processes identified herein are not correlated with local unfolding events identified in RNase H by denaturant-independent amide proton exchange (Chamberlain et al., 1996). Accordingly, the exchange processes observed in the present study most likely involve concerted conformational changes of the helices relative to the rest of the protein (the β-sheet), or of the helices relative to each other, that do not require breaking of intrahelical hydrogen bonds.

The complexity of eq 10 hinders analysis of chemical exchange in proteins because the populations and chemical shift differences for conformational states are usually unknown. As demonstrated herein, the temperature dependence of the exchange rate constants provides critical information on the time scale and activation energies for conformational exchange. The apparent chemical-exchange rate constants decrease as the temperature increases; consequently, the microscopic exchange rate constants must be greater than 2.7×10^3 s^{-1}. Assuming that $\Delta\omega < 2$ ppm, the upper bound for k_{ex} is ~10^5 s^{-1}. These estimates are consistent with the range of exchange rates of 10^5 to 10^4 s^{-1} measured by $R_{1\rho}$ experiments for the fibronectin type III domain of the protein tenascin (Akke & Palmer, 1996).

Conformational exchange processes in proteins have been studied using a variety of spectroscopic techniques. NMR spectroscopy has shown that 180° rotations (ring flips) of aromatic moieties in basic pancreatic trypsin inhibitor occur with apparent activation energies from 57 to >80 kJ/mol (Wagner, 1983). Recent measurements of the exchange rates of an interior water molecule in basic pancreatic trypsin inhibitor yield an apparent activation energy of ~90 kJ/mol (Denisov et al., 1996). Flash photolysis experiments of heme proteins indicate that motions underlying relaxation processes from photolyzed states have activation energies ranging from 6.3 ± 1.5 to 10 ± 1 kJ/mol (Steinbach et al., 1991). Activation energies for methyl rotations have been measured to be ~14 kJ/mol by NMR spectroscopy (Kowalewski, 1991). The apparent activation barriers observed for residues in RNase H range from ~20 to ~50 kJ/mol. Assuming that these barriers are underestimated by at most a factor of 2, the activation barriers are greater than activation energies for rotamer transitions and less than activation barriers for aromatic ring flips. Thus, the present results lie within physically reasonable bounds.

Despite the additional information available from the temperature dependence of R_{ex}, determining the actual microscopic exchange rates and the actual activation energies from CPMG experiments remains difficult. In principle, measurements of spin relaxation in the rotating frame by use of $R_{1\rho}$ experiments provide a superior approach because exchange rates and activation energies can be determined directly. The first residue-specific $R_{1\rho}$ studies of protein dynamics on microsecond to millisecond time scales have appeared recently (Szyperski et al., 1993; Akke & Palmer, 1996), and such techniques should permit more detailed investigation of conformational exchange dynamics in RNase H. Both CPMG and $R_{1\rho}$ methods rely on curve fitting to theoretical models for chemical exchange. Present experimental methods cannot discriminate between two-state and multiple-state exchange dynamics, and confounding effects of multiple conformational states are unknown. In addition, the NMR spectroscopic experiments do not elucidate the microscopic mechanism of conformational exchange; indeed, because exchange broadening results from time-dependent chemical shift perturbations, resonances of immobile nuclei can be broadened by dynamic effects propagated from nearby groups. The time scales of the conformational exchange processes observed for RNase H are many orders of magnitude slower than the time scales accessible by molecular dynamics simulations; therefore, interpretation of these and other data on chemical exchange in proteins presents new theoretical challenges.

Spectral Density Mapping. Spectral density mapping provides an alternative method for analyzing spin relaxation rate constants. Spectral density mapping does not require assumptions about the form of the rotational diffusion tensor of the molecule and does not depend on time scale separation

or extreme narrowing approximations implicit in the model-free formalisms. Consequently, spectral density mapping is a useful method particularly for disordered or highly flexible systems in which these assumptions are suspect. The simplicity of the spectral density analysis is counterbalanced by the difficulty in interpreting the resulting values of the spectral density function, particularly in the absence of data acquired at multiple magnetic field strengths. For example, the value of $J(0)$ obtained by spectral density mapping at a single magnetic field contains contributions from internal dynamics on fast time scales, chemical exchange, and overall rotational diffusion that cannot be easily separated. As shown in Figure 9, for a well-folded globular protein such as RNase H, the results of spectral density mapping are congruent with the results of the model-free analysis and consequently offer few advantages.

CONCLUSIONS

^{15}N nuclear spin relaxation has been used to characterize the intramolecular dynamics of *E. coli* RNase H at 285, 300, and 310 K. Over this temperature range, the generalized order parameters show a structure-dependent decrease, indicating slightly larger amplitudes of internal motion on picosecond to nanosecond time scales with increasing temperature, particularly for loop and terminal regions. The temperature dependence of the order parameters has been parametrized by a characteristic temperature that encapsulates the energy scale associated with the distribution of bond vector conformations. The characteristic temperatures suggest that secondary structures, loops, and termini populate a hierarchy of energy states. Few conformational states are thermally accessible for the backbone amides in secondary structures; consequently, librational contributions from these moieties to the heat capacity of the folded state of RNase H are quenched; in contrast, many conformational states are accessible for backbone amides in loops and termini. Effective internal correlation times are independent of temperature on both picosecond and nanosecond time scales and imply that, on these time scales, N−H bond vector dynamics occur within conformational energetic minima separated by low barriers (<5−10 kJ/mol). Chemical-exchange terms are decreased dramatically with increasing temperature, indicating both that the microscopic exchange rate is faster than the experimental CPMG pulsing rate and that microsecond time scale exchange phenomena in proteins are temperature activated with apparent activation barriers on the order of 20−50 kJ/mol. The reproducibility of the model-free parameters has been established by comparison with previous results for RNase H at 300 K (Mandel et al., 1995), and a potential conformational exchange process in the active site has been identified.

The present investigation is limited to a relatively narrow temperature range by the onset of thermal denaturation at high temperature (the T_m of RNase H is 52 °C) and by the increased line widths at low temperature due to the increased viscosity of water. Additional studies of motions in proteins over wider temperature ranges will be required to confirm and extend the results of the present investigation. Biological function and stability of proteins are strongly temperature dependent; the present results provide a first characterization of the effect of temperature on conformational dynamical modes in *E. coli* RNase H that may contribute to these phenomena.

ACKNOWLEDGMENT

Craig A. Bingman (Columbia University), David Fushman (Rockefeller University), Wayne A. Hendrickson (Columbia University), and Ann McDermott (Columbia University) are acknowledged gratefully for helpful discussions.

SUPPORTING INFORMATION AVAILABLE

Six tables giving relaxation parameters for *E. coli* RNase H at 285, 300, and 310 K (Tables S1−S3) and backbone dynamical parameters for *E. coli* RNase H at 285, 300, and 310 K (Tables S4−S6) (42 pages). Ordering information is given on any current masthead page.

REFERENCES

Abragam, A. (1961) *Principles of Nuclear Magnetism*, pp 1−599, Clarendon Press, Oxford.
Akke, M., & Palmer, A. G. (1996) *J. Am. Chem. Soc. 118*, 911−912.
Akke, M., Brüschweiler, R., & Palmer, A. G. (1993) *J. Am. Chem. Soc. 115*, 9832−9833.
Akke, M., Carr, P. A., & Palmer, A. G. (1994) *J. Magn. Reson., Ser. B 104*, 298−302.
Allerhand, A., & Gutowsky, H. S. (1965) *J. Chem. Phys. 42*, 1587−1599.
Barkhuijsen, H., de Beer, R., & van Ormondt, D. (1987) *J. Magn. Reson. 73*, 553−557.
Bloom, M., Reeves, L. W., & Wells, E. J. (1965) *J. Chem. Phys. 42*, 1615−1624.
Boyd, J., Hommel, U., & Campbell, I. D. (1990) *Chem. Phys. Lett. 175*, 477−482.
Brink, D. M., & Satchler, G. R. (1993) *Angular Momentum*, pp 1−170, Clarendon Press, Oxford.
Brüschweiler, R., & Wright, P. E. (1994) *J. Am. Chem. Soc. 116*, 8426−8427.
Brüschweiler, R., Liao, X., & Wright, P. E. (1995) *Science 268*, 886−889.
Cantor, R. C., & Schimmel, P. R. (1980) *Biophysical Chemistry*, pp 1−1371, W. H. Freeman, San Francisco.
Carr, H. Y., & Purcell, E. M. (1954) *Phys. Rev. 94*, 630−638.
Chamberlain, A. K., Handel, T. M., & Marqusee, S. (1996) *Nat. Struct. Biol. 3*, 782−787.
Champoux, J. J., Gilboa, E., & Baltimore, D. (1984) *J. Virol. 49*, 686−691.
Clore, G. M., Driscoll, P. C., Wingfield, P. T., & Gronenborn, A. M. (1990a) *Biochemistry 29*, 7387−7401.
Clore, G. M., Szabo, A., Bax, A., Kay, L. E., Driscoll, P. C., & Gronenborn, A. M. (1990b) *J. Am. Chem. Soc. 112*, 4989−4991.
Crouch, R. J. (1990) *New Biol. 2*, 771−777.
Crouch, R. J., & Dirksen, M.-L. (1982) in *Nuclease*, pp 211−241, Cold Spring Harbor Laboratory, Cold Spring Harbor, NY.
Dabora, J. M., & Marqusee, S. (1994) *Protein Sci. 3*, 1401−1408.
Davies, J. F., II, Hostomska, Z., Hostomsky, Z., Jordan, S. R., & Matthews, D. A. (1991) *Science 252*, 88−95.
Davis, D. G., Perlman, M. E., & London, R. E. (1994) *J. Magn. Reson., Ser. B 104*, 266−275.
de Massy, B., Fayet, O., & Kogoma, T. (1984) *J. Mol. Biol. 178*, 227−236.
Denisov, V. P., Peters, J., Hörlein, H. D., & Halle, B. (1996) *Nat. Struct. Biol. 3*, 505−509.
Doolittle, R. F., Feng, D. F., Johnson, M. S., & McClure, M. A. (1989) *Q. Rev. Biol. 64*, 1−30.
Farrow, N. A., Zhang, O., Szabo, A., Torchia, D. A., & Kay, L. E. (1995) *J. Biomol. NMR 6*, 153−162.
Frauenfelder, H., Parak, F., & Young, R. D. (1988) *Annu. Rev. Biophys. Biophys. Chem. 17*, 451−479.
Frauenfelder, H., Sligar, S. G., & Wolynes, P. G. (1991) *Science 254*, 1598−1603.
Furfine, E. S., & Reardon, J. E. (1991) *Biochemistry 30*, 7041−7046.
Garcia de la Torre, J., & Bloomfield, V. A. (1981) *Q. Rev. Biophys. 14*, 81−139.
Gilboa, E., Mitra, S. W., Goff, S., & Baltimore, D. (1979) *Cell 18*, 93−100.

Gurd, F. R. N., & Rothgeb, T. M. (1979) *Adv. Protein Chem. 33*, 73−165.
Hendrickson, W. A., Horton, J. R., & LeMaster, D. M. (1990) *EMBO J. 9*, 1665−1672.
Henry, E. R., & Szabo, A. (1985) *J. Chem. Phys. 82*, 4753−4761.
Hiyama, Y., Niu, C.-H., Silverton, J. V., Bavoso, A., & Torchia, D. A. (1988) *J. Am. Chem. Soc. 110*, 2378−2383.
Horiuchi, T., Maki, H., & Sekiguchi, M. (1984) *Mol. Gen. Genet. 195*, 17−22.
Huber, H. E., & Richardson, C. C. (1990) *J. Biol. Chem. 265*, 10565−10573.
Ishikawa, K., Nakamura, H., Morikawa, K., & Kanaya, S. (1993a) *Biochemistry 32*, 6171−6178.
Ishikawa, K., Nakamura, H., Morikawa, K., Kimura, S., & Kanaya, S. (1993b) *Biochemistry 32*, 7136−7142.
Ishikawa, K., Okumura, M., Katayanagi, K., Kimura, S., Kanaya, S., Nakamura, H., & Morikawa, K. (1993c) *J. Mol. Biol. 230*, 529−542.
Ishima, R., & Nagayama, K. (1995) *J. Magn. Reson., Ser. B 108*, 73−76.
Jen, J. (1978) *J. Magn. Reson. 30*, 111−128.
Kanaya, S., Kohara, A., Miura, Y., Sekiguchi, A., Iwai, S., Inoue, H., Ohtsuka, E., & Ikehara, M. (1990) *J. Biol. Chem. 265*, 4615−4621.
Katayanagi, K., Miyagawa, M., Matsushima, M., Ishikawa, S., Kanaya, S., Ikehara, M., Matsuzaki, T., & Morikawa, K. (1990) *Nature 347*, 306−309.
Katayanagi, K., Miyagawa, M., Matsushima, M., Ishikawa, M., Kanaya, S., Nakamura, H., Ikehara, M., Matsuzaki, T., & Morikawa, K. (1992) *J. Mol. Biol. 223*, 1029−1052.
Katayanagi, K., Ishikawa, M., Okumura, M., Ariyoshi, M., Kanaya, S., Kawano, Y., Suzuki, M., Tanaka, I., & Morikawa, K. (1993) *J. Biol. Chem. 268*, 22092−22099.
Kay, L. E., Nicholson, L. K., Delagio, F., Bax, A., & Torchia, D. A. (1992) *J. Magn. Reson. 97*, 359−375.
Kimura, S., Kanaya, S., & Nakamura, H. (1992a) *J. Biol. Chem. 267*, 22014−22017.
Kimura, S., Nakamura, H., Hashimoto, T., Oobatake, M., & Kanaya, S. (1992b) *J. Biol. Chem. 267*, 21535−21542.
Kitani, T., Yoda, K., Ogawa, T., & Okazaki, T. (1985) *J. Mol. Biol. 184*, 45−52.
Kördel, J., Skelton, N. J., Akke, M., Palmer, A. G., & Chazin, W. J. (1992) *Biochemistry 31*, 4856−4866.
Kowalewski, J. (1989) *Annu. Rep. NMR Spectrosc. 22*, 307−414.
Kowalewski, J. (1991) *Annu. Rep. NMR Spectrosc. 23*, 289−374.
Kraulis, P. J. (1991) *J. Appl. Crystallogr. 24*, 946−950.
Lee, L. K., Rance, M., Chazin, W. J., & Palmer, A. G. (1996) *J. Biomol. NMR* (in press).
Li, Y.-C., & Montelione, G. T. (1994) *J. Magn. Reson., Ser. B 105*, 45−51.
Lipari, G., & Szabo, A. (1982a) *J. Am. Chem. Soc. 104*, 4546−4559.
Lipari, G., & Szabo, A. (1982b) *J. Am. Chem. Soc. 104*, 4559−4570.
Luz, Z., & Meiboom, S. (1963) *J. Chem. Phys. 39*, 366−370.
Mandel, A. M., Akke, M., & Palmer, A. G. (1995) *J. Mol. Biol. 246*, 144−163.
Marion, D., Ikura, M., & Bax, A. (1989a) *J. Magn. Reson. 84*, 425−430.
Marion, D., Ikura, M., Tschudin, R., & Bax, A. (1989b) *J. Magn. Reson. 85*, 393−399.
Meiboom, S., & Gill, D. (1958) *Rev. Sci. Instrum. 29*, 688−691.
Messerle, B. A., Wider, G., Otting, G., Weber, C., & Wüthrich, K. (1989) *J. Magn. Reson. 85*, 608−613.
Mispelter, J., Lefevre, C., Adjadj, E., Quiniou, E., & Favaudon, V. (1995) *J. Biomol. NMR 5*, 233−244.
Mölling, K., Bolognesi, D. P., Bauer, H., Büsen, W., Plassmann, H. W., & Hausen, P. (1971) *Nat. New Biol. 234*, 240−243.
Muhandiram, D. R., Yamazaki, T., Sykes, B. D., & Kay, L. E. (1995) *J. Am. Chem. Soc. 117*, 11536−11544.
Nakamura, H., Oda, Y., Iwai, S., Inoue, H., Ohtsuka, E., Kanaya, S., Kimura, S., Katsuda, C., Katayanagi, K., Morikawa, K., Miyashiro, H., & Ikehara, M. (1991) *Proc. Natl. Acad. Sci. U.S.A. 88*, 11535−11539.
Nicholls, A., Sharp, K., & Honig, B. (1991) *Proteins: Struct., Funct., Genet. 11*, 281−296.
Nicholson, L. K., Kay, L. E., Baldisseri, D. M., Arango, J., Young, P. E., & Torchia, D. A. (1992) *Biochemistry 31*, 5253−5263.
Noggle, J. H., & Shirmer, R. E. (1971) *The Nuclear Overhauser Effect: Chemical Applications*, pp 1−259, Academic Press, New York.
Oda, Y., Nakamura, H., Kanaya, S., & Ikehara, M. (1991) *J. Biomol. NMR 1*, 247−255.
Oda, Y., Iwai, S., Ohtsuka, E., Ishikawa, M., Ikehara, M., & Nakamura, H. (1993a) *Nucleic Acids Res. 21*, 4690−4695.
Oda, Y., Yoshida, M., & Kanaya, S. (1993b) *J. Biol. Chem. 268*, 88−92.
Omer, C. A., & Faras, A. J. (1982) *Cell 30*, 797−805.
Palmer, A. G. (1993) *Curr. Opin. Biotechnol. 4*, 385−391.
Palmer, A. G., Rance, M., & Wright, P. E. (1991) *J. Am. Chem. Soc. 113*, 4371−4380.
Palmer, A. G., Skelton, N. J., Chazin, W. J., Wright, P. E., & Rance, M. (1992) *Mol. Phys. 75*, 699−711.
Palmer, A. G., Williams, J., & McDermott, A. (1996) *J. Phys. Chem. 100*, 13293−13310.
Peng, J. W., & Wagner, G. (1992) *J. Magn. Reson. 98*, 308−332.
Philippopoulos, M., & Lim, C. (1995) *J. Mol. Biol. 254*, 771−792.
Philippopoulos, M., Mandel, A. M., Palmer, A. G., & Lim, C. (1996) *Proteins: Struct., Funct., Genet.* (submitted for publication).
Shaka, A. J., Barker, P. B., & Freeman, R. (1985) *J. Magn. Reson. 64*, 547−552.
Skelton, N. J., Palmer, A. G., Akke, M., Kördel, J., Rance, M., & Chazin, W. J. (1993) *J. Magn. Reson., Ser. B 102*, 253−264.
Smith, J. S., & Roth, M. J. (1992) *J. Biol. Chem. 267*, 15071−15079.
Stein, H., & Hausen, P. (1969) *Science 166*, 393−395.
Steinbach, P. J., Ansari, A., Berendzen, J., Brauenstein, D., Chu, K., Cowen, B. R., Ehrenstein, D., Frauenfelder, H., Johnson, J. B., Lamb, D. C., Luck, S., Mourant, J. R., Nienhaus, G. U., Ormos, P., Philipp, R., Xie, A., & Young, R. D. (1991) *Biochemistry 30*, 3988−4001.
Studier, F. W., & Moffat, B. A. (1986) *J. Mol. Biol. 189*, 113−130.
Szyperski, T., Luginbühl, P., Otting, G., Güntert, P., & Wüthrich, K. (1993) *J. Biomol. NMR 3*, 151−164.
Tilton, R. F., Dewan, J. C., & Petsko, G. A. (1992) *Biochemistry 31*, 2469−2481.
Tjandra, N., Feller, S. E., Pastor, R. W., & Bax, A. (1995) *J. Am. Chem. Soc. 117*, 12562−12566.
Vold, R. L., Waugh, J. S., Klein, M. P., & Phelps, D. E. (1968) *J. Chem. Phys. 48*, 3831−3832.
Wagner, G. (1983) *Q. Rev. Biophys. 16*, 1−57.
Wagner, G. (1993) *Curr. Opin. Struct. Biol. 3*, 748−753.
Wand, A. J., Urbauer, J. L., McEvoy, R. P., & Bieber, R. J. (1996) *Biochemistry 35*, 6116−6125.
Wennerström, H. (1972) *Mol. Phys. 24*, 69−80.
Wintersberger, U. (1990) *Pharmacol. Ther. 48*, 259−280.
Yamazaki, T., Yoshida, M., & Nagayama, K. (1993) *Biochemistry 32*, 5656−5669.
Yamasaki, K., Ogasahara, K., Yutani, K., Oobatake, M., & Kanaya, S. (1995a) *Biochemistry 34*, 16552−16562.
Yamasaki, K., Saito, M., Oobatake, M., & Kanaya, S. (1995b) *Biochemistry 34*, 6587−6601.
Yang, D., & Kay, L. E. (1996) *J. Mol. Biol. 263*, 369−382.
Yang, W., Hendrickson, W. A., Crouch, R. J., & Satow, Y. (1990a) *Science 249*, 1398−1405.
Yang, W., Hendrickson, W. A., Kalman, E. T., & Crouch, R. J. (1990b) *J. Biol. Chem. 265*, 13553−13559.
Zheng, Z., Czaplicki, J., & Jardetzky, O. (1995) *Biochemistry 34*, 5212−5223.
Zhu, G., Torchia, D. A., & Bax, A. (1993) *J. Magn. Reson., Ser. A 105*, 219−222.

BI962089K